

Peer review status:

This is a non-peer-reviewed preprint submitted to EarthArXiv.

New insights into the cooling of the oceanic lithosphere from surface-wave tomographic inferences

Franck Latallerie¹, Paula Koelemeijer¹, Andrew Walker¹, Alessia Maggi²,
Sophie Lambotte², Christophe Zaroli²

¹Department of Earth Sciences, University of Oxford, Oxford, United Kingdom
²Institut Terre et Environement de Strasbourg, UMR7063, Université de Strasbourg, EOST/CNRS,
67084, Strasbourg CEDEX, France

Key Points:

- We present SS3DPacific: a new V_{SV} model of the Pacific ocean with 3D resolution and uncertainty
- We show that interpretations of oceanic lithosphere cooling are strongly biased by vertical resolution smearing
- An anomalous band-pattern aligned with fracture zones points to lateral complexities in the cooling of the oceanic lithosphere

Corresponding author: Paula Koelemeijer, paula.koelemeijer@earth.ox.ac.uk

Abstract

15

16

17

18

20

21

22

24 25

26

27

28

30

31

32

33

34

35

37

38

39

40

41

45

51

53

55

56

60

61

62

How oceanic plates cool and thicken with age remains a subject of debate, with several thermal models supported by apparently contradictory data. Combining a novel imaging technique that balances resolution and uncertainty with finite-frequency surface-wave measurements, we build tomographic model SS3DPacific to revisit the cooling style of the oceanic lithosphere beneath the Pacific ocean. Resolution analysis indicates a strong vertical smearing that biases estimates of the apparent lithospheric thickness, limiting the ability to discriminate between the half space and plate cooling models. Laterally, a pattern of anomalous bands in seismic velocity aligned with fracture zones points to additional lateral complexities in the lithosphere, complicating simple age-trend analyses.

Plain Language Summary

As the seafloor spreads away from mid-oceanic ridges, material cools down and the lithosphere, often defined by a temperature boundary, thickens. However, exactly how the lithosphere cools with age remains subject of debate. Some models suggest that it continues to cool down and thicken, others propose that the lower boundary of the lithosphere flattens due to secondary processes. Here, we investigate this problem using seismic imaging of the oceanic lithosphere. Our novel method allows us to assess quantitatively whether imaged structures are real or imaging artefacts. We show that imaging limitations do not allow us to discriminate between two widely-used models of the cooling of the oceanic lithosphere. Our results also show anomalous bands that line up with fractures in the oceanic crust. These point to lateral complexities in the cooling style of the oceanic lithosphere.

1 Introduction

Plate tectonics describes the motions of plates over the Earth's surface, with oceanic lithosphere being created at mid-oceanic ridges and sinking into the mantle in subduction zones. As oceanic plates move away from the ridges, they cool down by heat diffusion, subside, and thicken as evident in global bathymetry, heat flow, and gravity observations (Richardson et al., 1995; Richards et al., 2020). However, our understanding of the structure and evolution of oceanic plates remains simplified and subject of debate. Two heat diffusion models are often adopted for describing the thermal structure of the oceanic lithosphere: the Half-Space-Cooling (HSC) and Plate-Cooling (PC) models. HSC simply considers the lithosphere as a half-space cooling with age. While attractive for its simplicity, it does not match the apparent flattening of the lithosphere thickness at older ages supported by heat flow or bathymetry data. PC includes a boundary condition at depth that produces the apparent flattening (McKenzie, 1967; Parsons & Sclater, 1977). However, this ad hoc constraint assumes the existence of underlying physical processes that remain to be clarified (e.g. small-scale sub-lithospheric convection cells, Ballmer et al., 2009). Proponents of the HSC model reconcile it with observations either by adding complexity, such as secular cooling (e.g. Korenaga et al., 2021), or by calling attention to the inherent limitations of heat flow or bathymetry measurements (e.g. the effect of sediment layers, Richards et al., 2020) or uncertainty and resolution artifacts in seismic imaging (e.g. Rawlinson et al., 2014). New observations, with better uncertainty quantification, are required to address this problem.

Beyond the simple diffusive cooling of the lithosphere, bathymetry data show that oceanic plates are not smooth plates, but include great intraplate complexity (Figure 1), such as linear hotspot tracks, sea mounts and fracture zones. The effect of these structures on the thermal structure of the lithosphere remains unclear, and is at present poorly

accounted for in studies of the cooling of the lithosphere (Wessel & Haxby, 1990; Matthews et al., 2011).

Bathymetry, heat flow, gravity, seismic refraction and reflection data all provide crucial information for studying the oceanic lithosphere. However, constraints are either local or depth integrated and they are often strongly influenced by shallow Earth structure (e.g. crust and sediment cover). Surface-wave tomography is a complementary technique: surface waves are sensitive to temperature and offer global or basin-scale constraints (Ritzwoller et al., 2004; Zhou et al., 2006; Maggi et al., 2006; S. French et al., 2013; Auer et al., 2014; Isse et al., 2019). However, surface-wave data are contaminated by noise and theoretical errors, while seismic imaging is hindered by the heterogeneous source-receiver distribution and convoluted depth sensitivities. As a consequence, model resolution and uncertainty is often complex, but crucial to assess for robust interpretations (Rawlinson et al., 2014; Ritsema et al., 2007; Latallerie et al., 2022; Freissler et al., 2024). In practice, resolution and uncertainty are difficult to control, and computationally expensive to obtain for large-scale imaging problems (Fichtner & Trampert, 2011; An, 2012; Nolet et al., 1999; Ritsema & Lekić, 2020).

Here, we provide new constraints on the oceanic lithosphere using the 3D imaging framework of Latallerie et al. (2025). This approach combines the power of finite-frequency theory for surface waves (Snieder, 1986; Zhou, 2009a) with the Backus-Gilbert based SOLA method (Backus & Gilbert, 1968; Pijpers & Thompson, 1994; Zaroli, 2016) for inferring Earth structure. Finite-frequency offers a more accurate and fully three-dimensional one-step framework, while SOLA provides control on resolution and uncertainty, also making these readily available by construction. Using this approach, we develop SS3DPacific, a new 3D model of the vertically polarised shear-wave velocity (V_{SV}) for the Pacific uppermost mantle. Equipped with SS3DPacific, its 3D resolution and uncertainty, we revisit the age cooling trend of the lithosphere, and discuss our ability to discriminate between the HSC and PC models. Beyond the simple age dependence of lithospheric cooling, we also discuss further complexities in the structure of the lithosphere.

2 Data and method

We measure surface-wave phase-delays relative to 1D model STW105 (Kustowski et al., 2008) between 6 mHz and 21 mHz adopting the approach of Latallerie et al. (2025). To obtain measurement uncertainty estimates, we use a multi-taper technique. We select high-quality data based on a set of criteria, including spatial homogeneisation, resulting in a subset of 44,917 measurements (Figure 2a-b). The crustal signature is removed from the data using crustal model CRUST1.0 (Bassin et al., 2000).

We combine 3D finite-frequency theory and SOLA inferences, relating fundamental-mode Rayleigh-wave phase-delays measured on the vertical component to perturbations in V_{SV} , as described by Latallerie et al. (2025). Finite-frequency theory is more accurate than the great-circle approximation, and the volumetric nature of sensitivity kernels (Figure 2c) helps to stabilize the inversion (Zhou et al., 2004; Zhou, 2009a). Additionally, it allows us to image 3D structure in a single inversion step. We solve the inverse problem using the SOLA method (Zaroli, 2016; Zaroli et al., 2017), which provides control on resolution and uncertainty. The combination of finite-frequency theory with SOLA makes it possible to obtain resolution information in 3D, in contrast with earlier methods (e.g. Latallerie et al., 2022). We design a homogeneous target resolution throughout the model domain, aiming for a laterally isotropic resolution of 200 km in radius and 25 km vertically (e.g. pancake shape targets). We use a local parameterisation with voxels of $2^o \times 2^o \times 25$ km and invert only for cells where the data sensitivity (Figure 2d) is sufficiently large. For example, at 112 km depth, we invert only for voxels in which the data sensitivity is above ~ 10 rad.km⁻³.

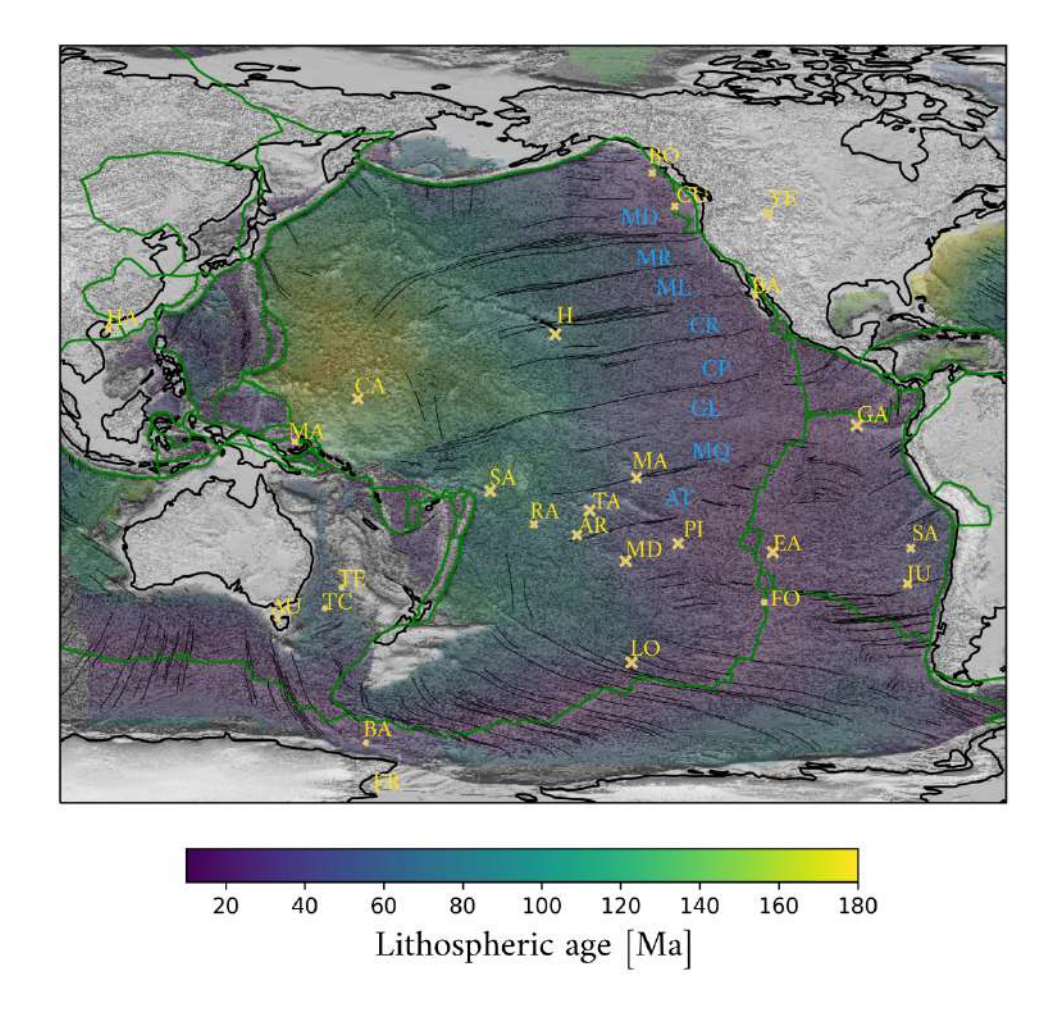


Figure 1. Map of the Pacific ocean and surrounding regions, showing the bathymetry (shaded background, from GEBCO Bathymetric Compilation Group 2024, 2024), lithospheric age (colormap, from Seton et al., 2020), hotpot locations (yellow crosses, from Jackson et al., 2021), fracture zones (black lines, from Matthews et al., 2011), and plate boundaries (green lines, from Bird, 2003). The size of the cross scales with the likelihood for the hotspot to have a deep plume origin, consistent with the scoring approach of Koppers et al. (2021). Fracture zones are labeled in blue (MD: Mendocino, MR: Murray, ML: Molokai, CR: Clarion, CP: Clipperton, GL: Galapagos, MQ: Marquesas, AT: Austral); and hotspots in yellow (BO: Bowie, GU: Guadeloupe, YE: Yellowstone, BA: Baja, GA: Galapagos, SA: San Felix, JU: Juan Fernandez, EA: Easter, FO: Foundation, LO: Louisville, ER: Erebus, BA: Baleny, AU: Australia, TC: Tasmanid Central, TE: Tasmanid Easter, MA: Manus, CA: Caroline, HA: Hanai, SA: Samoa, RA: Rarotonga, AR: Arago, TA: Tahiti, MD: Mac Donald, PI: Pitcairn, MA: Marquesas, H: Hawaii).

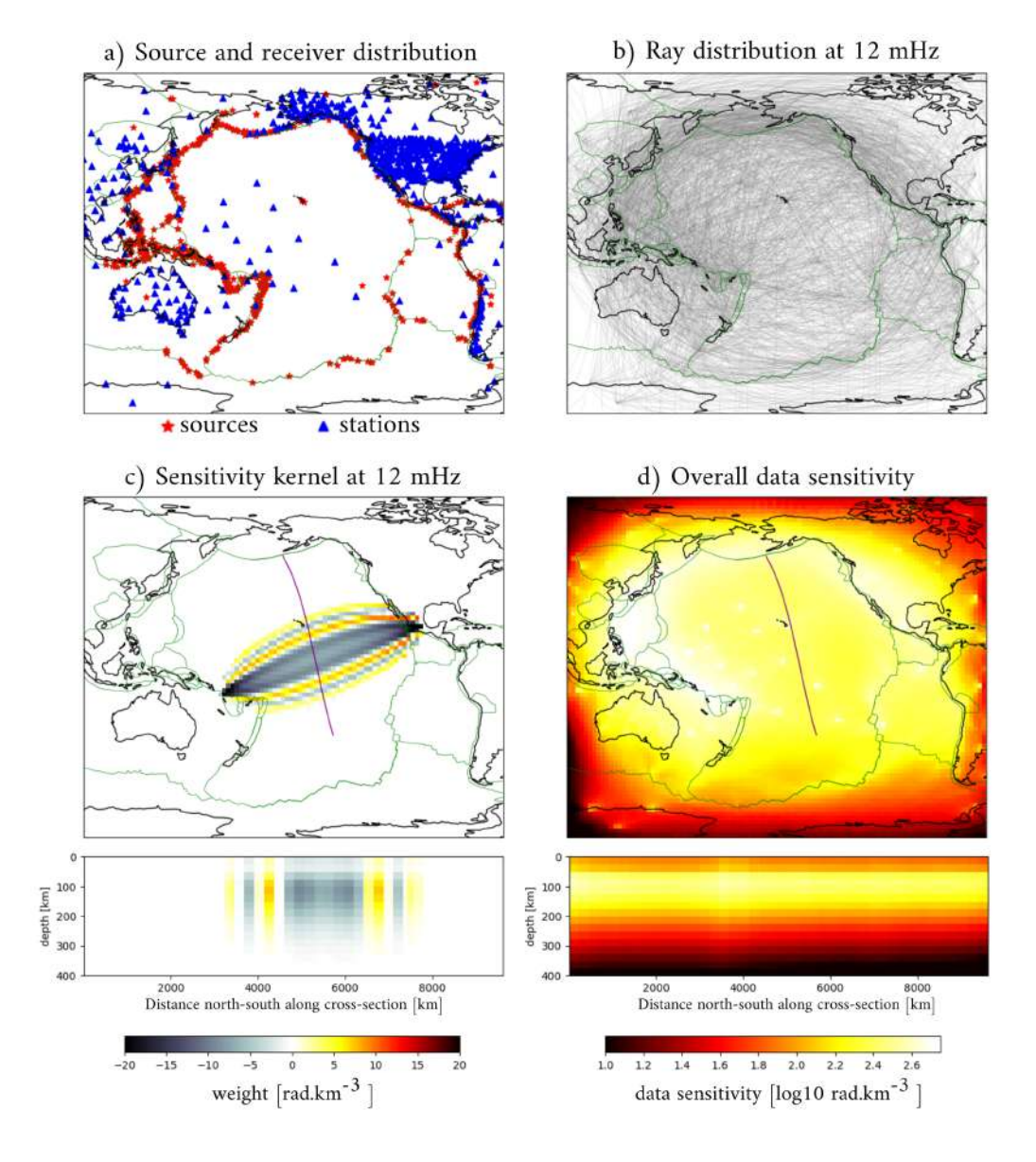


Figure 2. Data geometry and setup: a) Source and receiver distribution, b) Example ray distribution at 12 mHz, c) Example sensitivity kernel at 12 mHz including a cross-section along the purple line, d) Overall data sensitivity defined as $S_j = \log 10 \sum_i G_{ij}$, where G is the sensitivity matrix, with cross-section below. Maps of c) and d) are plotted at 112 km depth.

3 Structure, resolution and uncertainty of the Pacific uppermost mantle according to SS3DPacific

By construction, the SOLA method provides model uncertainty and resolution together with the model estimate of $\delta \ln V_{SV}$ (Figure 3 and 4). Counter-intuitively, uncertainty is higher in regions with good data coverage, balanced by a good fit to the target resolution in these areas. High uncertainty spikes co-locate with isolated stations where data sampling different paths contradict one another. Resolution is generally well-focused laterally and circular. The resolution length, defined here as the 1- σ contour of the Gaussian that best fits the resolving kernel, is around 300-500 km in radius. Vertically, the resolution tends to be smeared down to greater depths for shallow targets, or to shallower depths for deeper targets, with the optimal resolution found around 87-112 km depth. This strong vertical smearing, sometimes referred to as 'depth leakage', is expected to have strong implications for interpretations of the depth of structures in the tomographic model, and should therefore be taken into account.

SS3DPacific agrees well with other recent tomography models (detailed in Table S1) in terms of large-scale velocity anomalies, such as the location of cratons, mid-oceanic ridges and the velocity gradient with distance from ridges (Figure S1). We also observe a good correlation between hotspot locations and low-velocity anomalies that stand out after we remove the lithosphere cooling trend and mask velocity anomalies that are not significant (see Figure S2), following the approach of Latallerie et al. (2022).

4 Age cooling trend

To investigate the cooling trend of the uppermost mantle, we interpolate the lithospheric age model of Seton et al. (2020) onto the tomographic grid (Figure 3d) and use this to compute the averaged $\delta \ln V_{SV}$ of SS3DPacific and other tomography models in 2 Ma age bins (Figure 5). To avoid any complexities in the analysis, we analyse only cooling trends within the Pacific plate, far from plate boundaries, hotspots, and fracture zones (Figure S3). Following this procedure, we observe a wedge-like low-velocity region near the ridge that gradually deepens with age, before flattening (Figure 5), consistent with several other tomographic models.

We compare the trends of model SS3DPacific with predictions based on the HSC and PC models. For HSC, we compute the thermal structure using the analytical expression and constants from Stein and Stein (1992), whereas for PC we use the model of Richards et al. (2018). We apply the same age binning process as for the tomography. We do not convert temperatures to velocity to avoid assumptions in the conversion, and therefore only analyse the overall shape of the age trend and the impact of tomographic resolution on this. Throughout this analysis, we assume the $1175^{\circ}C$ isotherm represents the base of the lithosphere-asthenosphere boundary, as suggested by Richards et al. (2018).

To directly compare the observed and predicted age trends, we need to account for the limited tomographic resolution, e.g. 'tomographically filter' the temperature predictions. Our study is unique in that we can apply the resolution provided by SOLA to the HSC and PC predictions (solid lines in Figure 5 and Figure S4). This allows us to account for the vertical resolution smearing, which is crucial for interpreting structures such as the lithosphere-asthenosphere boundary. Figure 5 demonstrates that the filtering of HSC and PC predictions produces a similar isotherm 'wedge' shape as observed in the velocity structure of SS3DPacific. The filtering thus completely changes the geometry of the isotherms (i.e. cooling). Since this wedge-shape geometry of low-velocities is also present in other tomography models, these may also suffer from similar vertical resolution smearing. However, we cannot investigate this in detail, given full 3D resolution information is generally not available for other models.

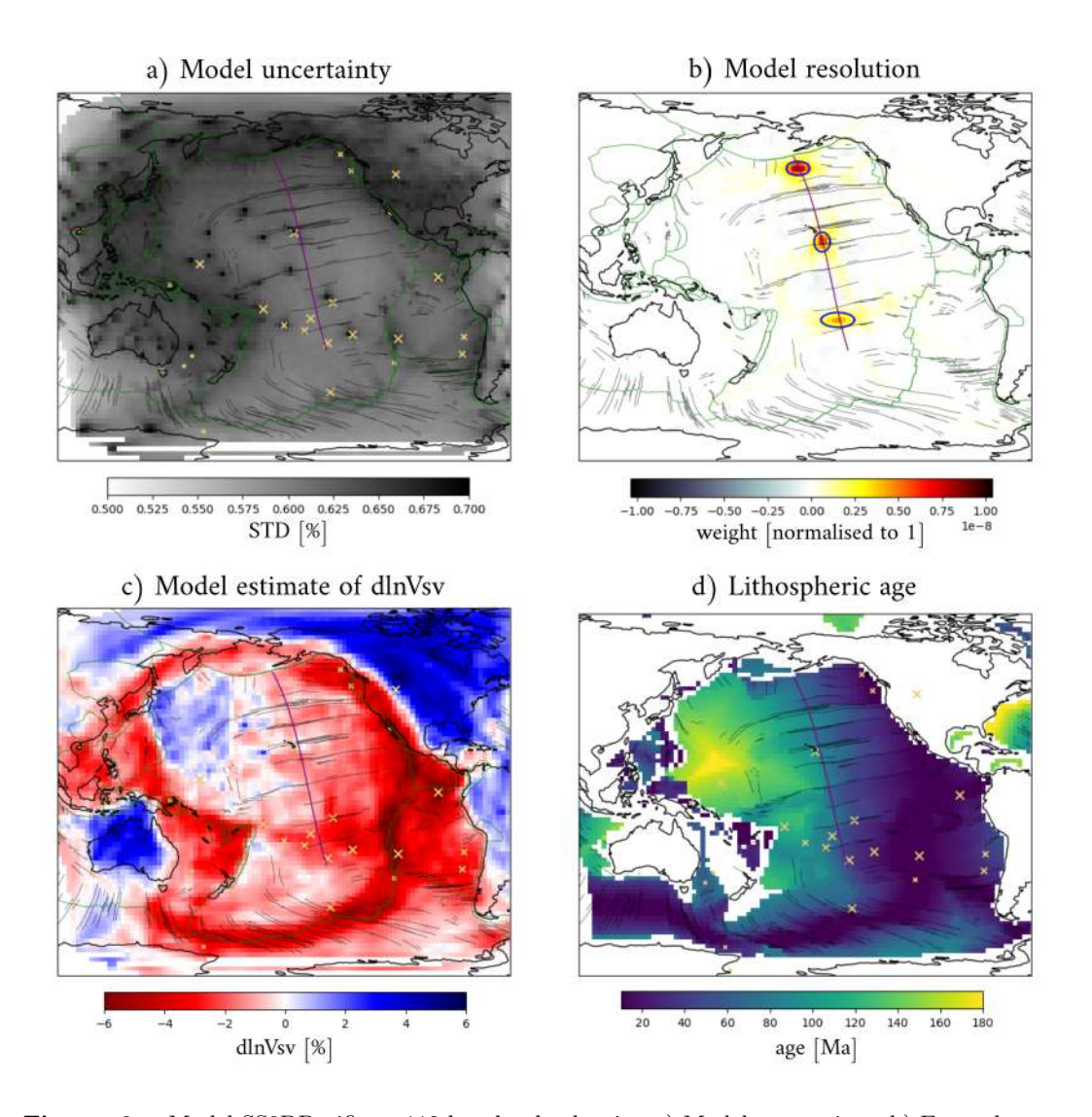
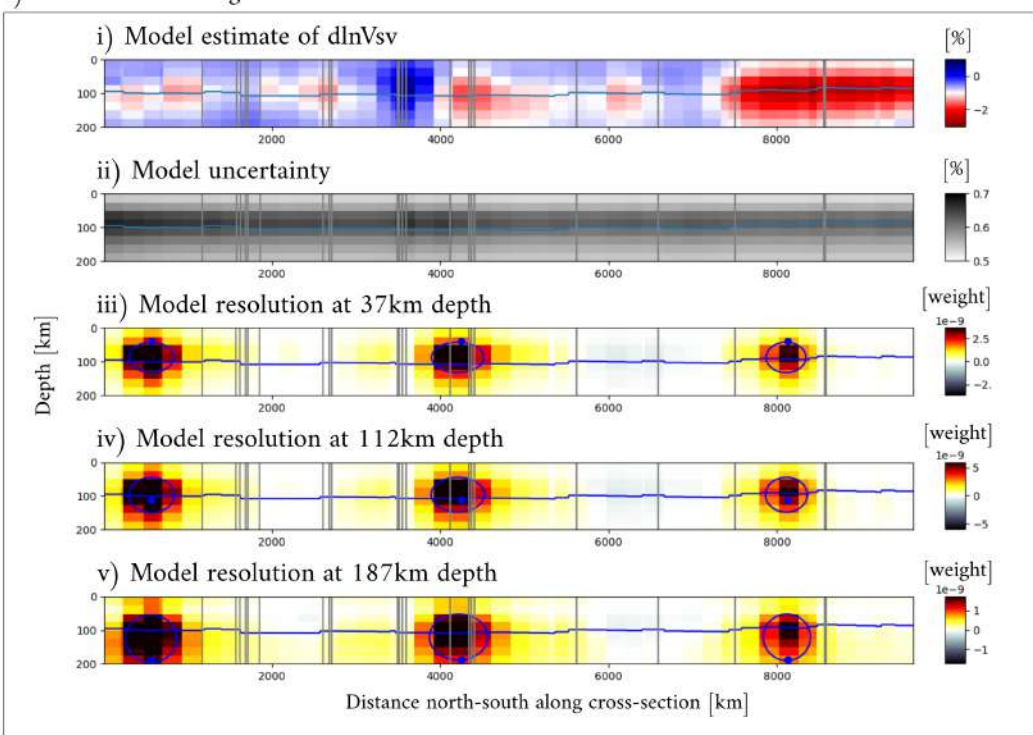


Figure 3. Model SS3DPacific at 112 km depth, showing a) Model uncertainty; b) Example resolution kernels for 3 selected locations; c) Model estimates of $\delta \ln V_{SV}$; and d) Age of the lithosphere in Ma. For the resolution kernels in b), the blue ellipses indicate the 1- σ contour of the best fitting Gaussian. The purple line indicates the location of the cross-sections shown in Figure 4.

a) Cross-section through SS3DPacific



b) Relationship between age and seismic velocity

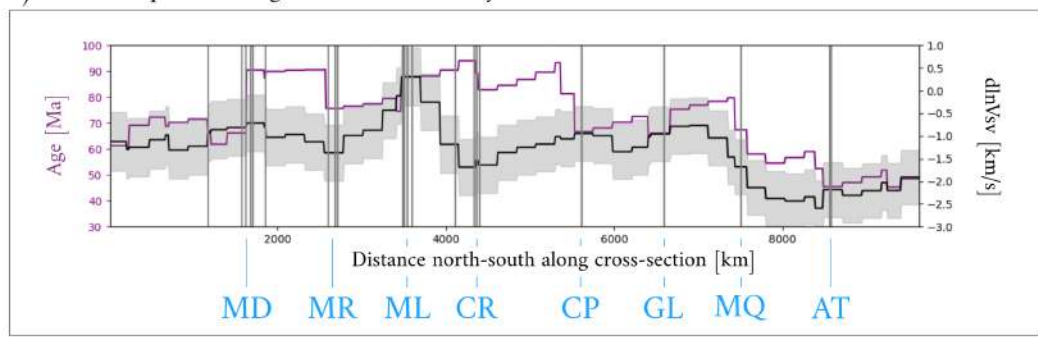


Figure 4. Model SS3DPacific compared to lithospheric age. a) Cross-sections through SS3DPacific along the purple line in Figure 3 showing i) Model estimate of $\delta \ln V_{SV}$, ii) Model uncertainty, iii-v) Example resolution kernels for target kernels centered at 37 km, 112 km, and 187 km depth respectively, at the same locations as in Figure 3b) as represented by blue dots. Blue ellipses indicate in each case the 1- σ contour of the best fitting Gaussian. The blue lines represent the depth of the 1175°C isotherm in the PC model. b) Lithospheric age (purple) compared to model estimate of $\delta \ln V_{SV}$ at 112 km depth (black line with grey bands representing the 1- σ uncertainty). The vertical grey lines show the location of the main fracture zones, labeled in blue (see Figure 1).

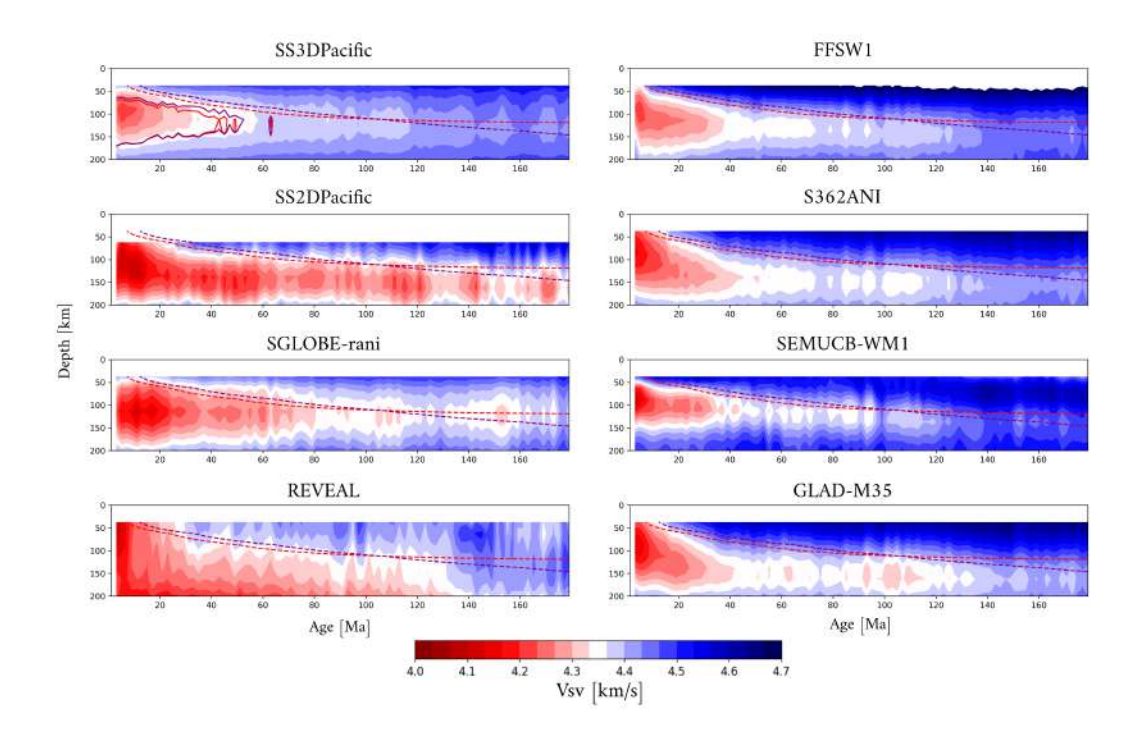


Figure 5. V_{SV} structure of SS3DPacific compared to other seismic tomography models, averaged in 2 Ma age bins. Purple and red dashed lines represent the 1175° C isotherm of the HSC and PC models, respectively. For SS3DPacific, we also include the filtered versions that account for the limited resolution (solid lines). We include tomography models SS2DPacific (Latallerie et al., 2022), SGLOBE-rani (Chang et al., 2015), REVEAL (Thrastarson et al., 2024), FFSW1 (Zhou et al., 2006), S362ANI (Kustowski et al., 2008), SEMUCB-WM1 (S. W. French & Romanowicz, 2014), and GLAD-M35 (Cui et al., 2024).

While the difference between the original predictions of the HSC and PC models (dashed lines) is small, filtering makes them appear even more similar (solid lines). This implies that discriminating between them using surface-wave tomography is difficult (Figure S4). In particular, the flattening with age of the PC model appears weaker after filtering, diminishing the diagnostic difference between the HSC and PC models. Therefore, vertical resolution smearing in surface-wave tomography is vital to take into account when interpreting imaged structures in terms of lithospheric cooling.

5 Fracture zones

Besides the main features in SS3DPacific (see Section 3), we observe an interesting pattern of anomalous bands aligned with major fracture zones in the North West and Equatorial Pacific (see Figures 3 and 4i). This is most pronounced around the depth of the lithosphere-asthenosphere boundary as predicted by the $1175^{\circ}C$ isotherm of the PC model. The peak-to-peak difference in $\delta \ln V_{SV}$ between the bands is $\sim 3\%$, which is above the average model uncertainty in this region of $\sim 0.7\%$ (Figure 4ii). The bands are spaced roughly ~ 800 km apart, thus resolvable given the lateral resolution length of ~ 450 km in this region (Figure 4iii-v). The resolution is laterally also very isotropic here (Figure 3b), implying that these bands do not arise from a lateral resolution smearing effect. As we applied crustal corrections on the data, it is also unlikely to arise from a leakage of crustal structure down to the upper mantle. To further reinforce this argument, we repeat our

SOLA inferences for $\delta \ln V_{SV}$ structure without the crustal correction, as well as for $\delta \ln V_{SV}$ structure that only arises from the crustal correction term (Figure S5). The banded pattern is already visible in the model without crustal correction (Figure S5a). Our tests indicate that the banded pattern is not introduced or reinforced by the crustal correction (Figure S5b). However, the crust could still cause the bands if the crustal model, or the crustal correction strategy, is insufficient for removing the crustal effect.

To the best of our knowledge, this banded pattern at lithosphere-asthenosphere boundary depths has not been seen or interpreted in existing tomography models (Figure S1). We argue that we can resolve it in SS3DPacific thanks to the combined use of finite-frequency theory and SOLA inferences. The detailed sensitivity in the volumetric sensitivity kernels (Figure 2c) adds physical information, explaining why we are able to obtain a coherent Pacific-wide model with only 44,917 measurements, compared with state-of-theart surface-wave tomography studies that typically use millions of measurements. The SOLA method is also able to extract relevant information from the data at every target location. Particularly, by designing the target kernels, we have prioritized a larger, but isotropic resolution over a smaller, but highly anisotropic and complex resolution.

Models for the cooling of the lithosphere usually assume a laterally infinite plate, only accounting for vertical diffusion of heat. Scaling analysis indicates that lateral diffusion in the direction of plate motion can be neglected (Parsons & Sclater, 1977), and that no diffusion is expected perpendicular to this if the temperature is constant. However, fracture zones produce lateral offsets in lithospheric age and thus thermal structure that are likely incompatible with these assumptions. This may explain the bands of low and high velocity that we observe in SS3DPacific. Further investigation of this would require a numerical model of the thermal structure including offsets in the lithospheric age, and a comparison of predictions from this model to the banded pattern observed in SS3DPacific. In turn, the tomographic observations could be used as new constraints on the parameters of such modeling of the oceanic lithosphere.

In the southern part of the cross-section (Figure 4), the anomalous bands appear to follow a consistent, expected relationship between age and wavespeed (younger lithosphere being slower and older lithosphere being faster). However, in the northern part (between the Mendocino and Clipperton fracture zones), we note a more complex relationship. While uncertainty and resolution limit our ability to interpret these trends, it suggests that additional non-negligible physical processes may occur at the fracture zones themselves. This is supported by other work that suggests that important changes in the structure of the lithosphere might occur at fracture zones. For example, the nature of volcanism along volcanic arcs has been observed to vary above subducted fracture zones (Manea et al., 2014), fracture zones appear to be more seismically active than thought (Bohnenstiehl et al., 2004), and may have higher heat flow than the average oceanic domain (Gregory et al., 2023). More relevant to this work, they may be subject to fluid movements, hydration, metasomatism and water induced melting (Schmeling et al., 2017), potentially leading to local thinning of the lithosphere (Wang et al., 2022). While these processes occur on shorter spatial scales than SS3DPacific can resolve, the observed banded pattern in $\delta \ln V_{SV}$ also hints at complexities in the structure of the lithosphere across fracture zones.

6 Discussion and concluding remarks

The availability of resolution and uncertainties allows us to quantitatively assess the robustness of different features and to compare SS3DPacific to model predictions of lithospheric cooling. Resolution analysis shows that it is impossible to discriminate between the HSC and PC models due to strong vertical resolution smearing, a limitation that is likely shared with other surface-wave tomography models. A clear step forward would be the inclusion of overtones in our methodology, to better illuminate deeper man-

tle structure and thus potentially reduce the vertical resolution smearing. While some other tomography models do include overtone data (see Table S1), in the absence of resolution information for these, it is difficult to assess at present whether these data reduce the vertical resolution smearing sufficiently to discriminate between the two cooling models.

Laterally, SS3DPacific features a pattern of anomalous bands aligned with oceanic fracture zones that produce offsets in the age of the lithosphere. These bands do not show the expected relationship between age and wavespeed everywhere, suggesting that lateral heat transfer may occur. Thermal modeling including lateral heat diffusion across fracture zones would help to understand these observations better, which in turn could provide new constraints on the physical characteristics of the lithosphere. Particularly, not all fracture zones have the same seismic signature; some align with velocity lows, others with velocity highs, reflecting possibly that different mechanisms occur at the fracture zones themselves. If fracture zones represented pathways for fluids, such as melt or water, the lithosphere along fracture zones may reheat and be rejuvenated or undergo cooling and metasomatism, respectively.

To better investigate the processes occurring at fracture zones, new seismic constraints could be derived using the same approach as presented here. In particular, mapping both Vp and Vs with the same local resolution (Serra et al., 2025; Restelli et al., 2024) to obtain robust V_P/V_S ratios could provide constraints on enrichment in serpentine along fracture zones. Imaging radial anisotropy through joint inversion of Love and Rayleigh waves would also provide constraints on fracture alignments along fracture zones. Finally, mapping attenuation would make it possible to map melt migration across the fracture zones.

The age-dependent structure of the oceanic lithosphere remains to be explored. Lateral complexities in lithospheric structure indicate that lateral diffusion of heat may play a significant role across fracture zones. Detailed seismological images with better resolution (laterally and vertically) will be needed to unravel the complex cooling history of the oceanic lithosphere. Such images will have to be accompanied by robust uncertainty and resolution information to ensure interpretations are free from methodological biases.

Conflict of interest

The authors declare no conflict of interest relevant to this study.

Acknowledgments

This research was supported by the UKRI NERC Large grant "Mantle Circulation Constrained (MC2): A multidisciplinary 4D Earth framework for understanding mantle upwellings" (NE/T01248X/1, NE/T012684/1, and NE/T01684/1). FL and PK also acknowledge financial support from the Royal Society (URF\R1\180377 and RF\ERE\231085). CZ acknowledges financial support from ITES (Institut Terre et Environnement de Strasbourg, UMR 7063) for a research visit to Oxford. This study used the ARCHER2 UK National Supercomputing Service (https://www.archer2.ac.uk). For the purpose of open access, the authors have applied a CC BY public copyright license to any Author Accepted Manuscript version arising.

Data and code availability

Seismic source solutions were downloaded from the Global Centroid Moment Tensor (GCMT) Catalog (Dziewonski et al., 1981; Ekström et al., 2012). The facilities of

the EarthScope Consortium were used to access waveforms and related metadata and derived data products. These services are funded through the National Science Foundation's Seismological Facility for the Advancement of Geoscience (SAGE) Award under Cooperative Agreement EAR-1724509. Citations for networks used are provided in the supplementary information.

To compute the finite-frequency sensitivity kernels, we used software provided by Ying Zhou (Zhou, 2009b), available via their webpage (http://seismo.geos.vt.edu/software.html). To compute the reference seismograms in a 1D radial Earth model, we used normal modes summation as implemented in MINEOS 1.0.2 (Masters et al., 2011) published under the GPL2 license. We thank the Computational Infrastructure for Geodynamics (http://geodynamics.org), which is funded by the National Science Foundation under awards EAR-0949446, EAR-1550901, and EAR-2149126, for making the code available.

The SOLA tomography code used in this study consists of running the LSQR algorithm of Paige and Saunders (1982) with specific input matrices and vectors. These inputs can be constructed from the sensitivity matrix and target kernels as detailed in Appendix A1 of (Zaroli, 2016). The LSQR code is freely downloadable from the webpage of the Systems Optimisation Laboratory (Stanford University): https://web.stanford.edu/group/SOL/software/lsqr/. A pre-constructed software package for finite-frequency surface-wave SOLA tomography is available at https://doi.org/10.5281/zenodo.14847404.

We made extensive use of Ubuntu 20.04.6 LTS (Canonical Ltd, 2024), and Python packages Numpy (Harris et al., 2020), Scipy (Virtanen et al., 2020), Pandas (team, 2020), and Matplotlib (Hunter, 2007).

The surface-wave phase-delay measurements, SS3DPacific model files, and plotting scripts are available at http://data.bgs.ac.uk/id/dataHolding/13608405.

References

- An, M. (2012, November). A simple method for determining the spatial resolution of a general inverse problem. Geophysical Journal International, 191(2), 849–864. Retrieved 2022-02-02, from https://academic.oup.com/gji/article/191/2/849/646030 doi: 10.1111/j.1365-246X.2012.05661.x
- Auer, L., Boschi, L., Becker, T. W., Nissen-Meyer, T., & Giardini, D. (2014, April). Savani: A variable resolution whole-mantle model of anisotropic shear velocity variations based on multiple data sets. Journal of Geophysical Research: Solid Earth, 119(4), 3006-3034. Retrieved 2021-01-26, from http://doi.wiley.com/10.1002/2013JB010773 doi: 10.1002/2013JB010773
- Backus, G., & Gilbert, F. (1968, October). The Resolving Power of Gross Earth Data. Geophysical Journal International, 16(2), 169–205. Retrieved 2020-08-04, from https://academic.oup.com/gji/article-lookup/doi/10.1111/j.1365-246X.1968.tb00216.x doi: 10.1111/j.1365-246X.1968.tb00216.x
- Ballmer, M. D., van Hunen, J., Ito, G., Bianco, T. A., & Tackley, P. J. (2009, June). Intraplate volcanism with complex age-distance patterns: A case for small-scale sublithospheric convection: INTRAPLATE VOLCANISM FROM SMALL-SCALE CONVECTION. Geochemistry, Geophysics, Geosystems, 10(6), n/a-n/a. Retrieved 2021-06-16, from http://doi.wiley.com/10.1029/2009GC002386 doi: 10.1029/2009GC002386
- Bassin, C., Laske, G., & Masters, G. (2000). The Current Limits of Resolution for Surface Wave Tomography in North America. *Eos, Transactions American Geophysical Union*, 81 (F897).
- Bird, P. (2003, March). An updated digital model of plate boundaries: UPDATED MODEL OF PLATE BOUNDARIES. Geochemistry, Geophysics, Geosys-

tems, 4(3). Retrieved 2022-10-12, from http://doi.wiley.com/10.1029/2001GC000252 doi: 10.1029/2001GC000252

- Bohnenstiehl, D. R., Tolstoy, M., & Chapp, E. (2004, January). Breaking into the plate: A 7.6 Mw fracture-zone earthquake adjacent to the Central Indian Ridge. Geophysical Research Letters, 31(2), 2003GL018981. Retrieved 2025-08-23, from https://agupubs.onlinelibrary.wiley.com/doi/10.1029/2003GL018981 doi: 10.1029/2003GL018981
- Chang, S.-J., Ferreira, A. M. G., Ritsema, J., van Heijst, H. J., & Woodhouse, J. H. (2015, June). Joint inversion for global isotropic and radially anisotropic mantle structure including crustal thickness perturbations: RADIALLY ANISOTROPIC MANTLE STRUCTURE. Journal of Geophysical Research: Solid Earth, 120(6), 4278–4300. Retrieved 2023-02-06, from http://doi.wiley.com/10.1002/2014JB011824 doi: 10.1002/2014JB011824
- Cui, C., Lei, W., Liu, Q., Peter, D., Bozdağ, E., Tromp, J., ... Pugmire, D. (2024, August). GLAD-M35: a joint P and S global tomographic model with uncertainty quantification. Geophysical Journal International, 239(1), 478–502. Retrieved 2025-07-18, from https://academic.oup.com/gji/article/239/1/478/7727823 (Publisher: Oxford University Press (OUP)) doi: 10.1093/gji/ggae270
- Dziewonski, A. M., Chou, T.-A., & Woodhouse, J. H. (1981, April). Determination of earthquake source parameters from waveform data for studies of global and regional seismicity. *Journal of Geophysical Research: Solid Earth*, 86(B4), 2825–2852. Retrieved 2022-09-15, from http://doi.wiley.com/10.1029/JB086iB04p02825 doi: 10.1029/JB086iB04p02825
- Ekström, G., Nettles, M., & Dziewoński, A. (2012, June). The global CMT project 2004-2010: Centroid-moment tensors for 13,017 earthquakes. *Physics of the Earth and Planetary Interiors*, 200-201, 1-9. Retrieved 2022-08-08, from https://linkinghub.elsevier.com/retrieve/pii/S0031920112000696 doi: 10.1016/j.pepi.2012.04.002
- Fichtner, A., & Trampert, J. (2011, December). Resolution analysis in full waveform inversion: Resolution in full waveform inversion. Geophysical Journal International, 187(3), 1604–1624. Retrieved 2023-10-04, from https://academic.oup.com/gji/article-lookup/doi/10.1111/j.1365-246X.2011.05218.x doi: 10.1111/j.1365-246X.2011.05218.x
- Freissler, R., Schuberth, B. S. A., & Zaroli, C. (2024, May). A concept for the global assessment of tomographic resolution and uncertainty. Geophysical Journal International, ggae178. Retrieved 2024-05-31, from https://academic.oup.com/gji/advance-article/doi/10.1093/gji/ggae178/7680010 doi: 10.1093/gji/ggae178
- French, S., Lekic, V., & Romanowicz, B. (2013, October). Waveform Tomography Reveals Channeled Flow at the Base of the Oceanic Asthenosphere. Science, 342 (6155), 227-230. Retrieved 2020-08-04, from https://www.sciencemag.org/lookup/doi/10.1126/science.1241514 doi: 10.1126/science.1241514
- French, S. W., & Romanowicz, B. A. (2014, December). Whole-mantle radially anisotropic shear velocity structure from spectral-element waveform tomography. Geophysical Journal International, 199(3), 1303–1327. Retrieved 2022-10-09, from http://academic.oup.com/gji/article/199/3/1303/612270/Wholemantle-radially-anisotropic-shear-velocity doi: 10.1093/gji/ggu334
- GEBCO Bathymetric Compilation Group 2024. (2024). The GEBCO_2024

 Grid a continuous terrain model of the global oceans and land. NERC

 EDS British Oceanographic Data Centre NOC. Retrieved 2025-0721, from https://www.bodc.ac.uk/data/published_data_library/
 catalogue/10.5285/1c44ce99-0a0d-5f4f-e063-7086abc0ea0f/ doi:

10.5285/1C44CE99-0A0D-5F4F-E063-7086ABC0EA0F

- Gregory, E. P. M., Villinger, H., Singh, S. C., & Kaul, N. (2023, April). High Heat Flow Anomaly Within the St Paul Fracture Zone: Heat Advection and/or Inherent Thermal Structure? Geochemistry, Geophysics, Geosystems, 24(4), e2022GC010385. Retrieved 2025-06-12, from https://agupubs.onlinelibrary.wiley.com/doi/10.1029/2022GC010385 doi: 10.1029/2022GC010385
 - Harris, C. R., Millman, K. J., Walt, S. J. v. d., Gommers, R., Virtanen, P., Cournapeau, D., ... Oliphant, T. E. (2020, September). Array programming with NumPy. Nature, 585 (7825), 357–362. Retrieved from https://doi.org/10.1038/s41586-020-2649-2 (Publisher: Springer Science and Business Media LLC) doi: 10.1038/s41586-020-2649-2
 - Hunter, J. D. (2007). Matplotlib: A 2D graphics environment. *Computing in Science & Engineering*, 9(3), 90–95. (Publisher: IEEE COMPUTER SOC) doi: 10.1109/MCSE.2007.55
 - Isse, T., Kawakatsu, H., Yoshizawa, K., Takeo, A., Shiobara, H., Sugioka, H., ... Reymond, D. (2019, March). Surface wave tomography for the Pacific Ocean incorporating seafloor seismic observations and plate thermal evolution. *Earth and Planetary Science Letters*, 510, 116–130. Retrieved 2020-08-04, from https://linkinghub.elsevier.com/retrieve/pii/S0012821X19300032 doi: 10.1016/j.epsl.2018.12.033
 - Jackson, M. G., Becker, T. W., & Steinberger, B. (2021, March). Spatial Characteristics of Recycled and Primordial Reservoirs in the Deep Mantle. Geochemistry, Geophysics, Geosystems, 22(3), e2020GC009525. Retrieved 2025-06-19, from https://agupubs.onlinelibrary.wiley.com/doi/10.1029/2020GC009525 doi: 10.1029/2020GC009525
 - Koppers, A. A. P., Becker, T. W., Jackson, M. G., Konrad, K., Müller, R. D., Romanowicz, B., ... Whittaker, J. M. (2021, May). Mantle plumes and their role in Earth processes. Nature Reviews Earth & Environment, 2(6), 382-401. Retrieved 2024-11-05, from https://www.nature.com/articles/s43017-021-00168-6 doi: 10.1038/s43017-021-00168-6
 - Korenaga, T., Korenaga, J., Kawakatsu, H., & Yamano, M. (2021, June). A New Reference Model for the Evolution of Oceanic Lithosphere in a Cooling Earth. Journal of Geophysical Research: Solid Earth, 126(6), e2020JB021528. Retrieved 2025-06-23, from https://agupubs.onlinelibrary.wiley.com/doi/10.1029/2020JB021528 doi: 10.1029/2020JB021528
 - Kustowski, B., Ekström, G., & Dziewoński, A. M. (2008, June). Anisotropic shearwave velocity structure of the Earth's mantle: A global model. *Journal of Geophysical Research*, 113(B6), B06306. Retrieved 2022-10-03, from http://doi.wiley.com/10.1029/2007JB005169 doi: 10.1029/2007JB005169
 - Latallerie, F., Zaroli, C., Lambotte, S., & Maggi, A. (2022, April). Analysis of tomographic models using resolution and uncertainties: a surface wave example from the Pacific. *Geophysical Journal International*, 230(2), 893–907. Retrieved 2022-04-20, from https://academic.oup.com/gji/article/230/2/893/6544670 doi: 10.1093/gji/ggac095
 - Latallerie, F., Zaroli, C., Lambotte, S., Maggi, A., Walker, A., & Koelemeijer, P. (2025, August). Towards surface wave tomography with 3D resolution and uncertainty: Resolution-uncertainty in 3D surface-wave tomography. Seismica, 4(2). Retrieved 2025-09-02, from https://seismica.library.mcgill.ca/article/view/1407 doi: 10.26443/seismica.v4i2.1407
- Maggi, A., Debayle, E., Priestley, K., & Barruol, G. (2006, September). Multimode surface waveform tomography of the Pacific Ocean: a closer look at the lithospheric cooling signature. Geophysical Journal International, 166(3), 1384–1397. Retrieved 2020-08-04, from https://academic.oup.com/gji/article-lookup/doi/10.1111/j.1365-246X.2006.03037.x doi:

10.1111/j.1365-246X.2006.03037.x

- Manea, V. C., Leeman, W. P., Gerya, T., Manea, M., & Zhu, G. (2014, October). Subduction of fracture zones controls mantle melting and geochemical signature above slabs. *Nature Communications*, 5(1). Retrieved 2025-07-17, from https://www.nature.com/articles/ncomms6095 (Publisher: Springer Science and Business Media LLC) doi: 10.1038/ncomms6095
- Masters, G., Woodhouse, J. H., & Freeman, G. (2011). *Mineos v1.0.2.* Computational Infrastructure for Geodynamics. Retrieved from https://geodynamics.org/cig,2011.
- Matthews, K. J., Müller, R. D., Wessel, P., & Whittaker, J. M. (2011, December). The tectonic fabric of the ocean basins. *Journal of Geophysical Research*, 116(B12), B12109. Retrieved 2025-06-12, from http://doi.wiley.com/10.1029/2011JB008413 doi: 10.1029/2011JB008413
- McKenzie, D. P. (1967, December). Some remarks on heat flow and gravity anomalies. *Journal of Geophysical Research*, 72(24), 6261–6273. Retrieved 2025–07-21, from http://doi.wiley.com/10.1029/JZ072i024p06261 (Publisher: American Geophysical Union (AGU)) doi: 10.1029/jz072i024p06261
- Nolet, G., Montelli, R., & Virieux, J. (1999, July). Explicit, approximate expressions for the resolution and a posteriori covariance of massive tomographic systems. Geophysical Journal International, 138(1), 36-44. Retrieved 2022-10-10, from https://academic.oup.com/gji/article-lookup/doi/10.1046/j.1365-246x.1999.00858.x doi: 10.1046/j.1365-246x.1999.00858.x
- Paige, C. C., & Saunders, M. A. (1982, March). LSQR: An Algorithm for Sparse Linear Equations and Sparse Least Squares. ACM Transactions on Mathematical Software (TOMS), 8(1), 43-71. Retrieved 2020-08-04, from http://dl.acm.org/doi/10.1145/355984.355989 doi: 10.1145/355984.355989
- Parsons, B., & Sclater, J. G. (1977, February). An analysis of the variation of ocean floor bathymetry and heat flow with age. Journal of Geophysical Research, 82(5), 803–827. Retrieved 2020-08-04, from http://doi.wiley.com/10.1029/JB082i005p00803 doi: 10.1029/JB082i005p00803
- Pijpers, F. P., & Thompson, M. J. (1994, January). The SOLA method for helioseismic inversion. *Astronomy and Astrophysics*, 281, 231–240. Retrieved 2024-08-20, from https://ui.adsabs.harvard.edu/abs/1994A&A...281..231P (ADS Bibcode: 1994A&A...281..231P)
- Rawlinson, N., Fichtner, A., Sambridge, M., & Young, M. (2014). Seismic Tomography and the Assessment of Uncertainty. *Advances in Geophysics*, 55, 1-76. Retrieved from https://www.sciencedirect.com/science/article/pii/S0065268714000028 doi: https://doi.org/10.1016/bs.agph.2014.08.001.
- Restelli, F., Zaroli, C., & Koelemeijer, P. (2024, February). Robust estimates of the ratio between S- and P-wave velocity anomalies in the Earth's mantle using normal modes. *Physics of the Earth and Planetary Interiors*, 347, 107135. Retrieved 2024-04-03, from https://linkinghub.elsevier.com/retrieve/pii/S0031920123001619 doi: 10.1016/j.pepi.2023.107135
- Richards, F., Hoggard, M., Cowton, L. R., & White, N. (2018, October). Reassessing the Thermal Structure of Oceanic Lithosphere With Revised Global Inventories of Basement Depths and Heat Flow Measurements. *Journal of Geophysical Research: Solid Earth*, 123(10), 9136–9161. Retrieved 2025-02-28, from https://agupubs.onlinelibrary.wiley.com/doi/10.1029/2018JB015998 doi: 10.1029/2018JB015998
- Richards, F., Hoggard, M., Crosby, A., Ghelichkhan, S., & White, N. (2020, December). Structure and dynamics of the oceanic lithosphere-asthenosphere system. Physics of the Earth and Planetary Interiors, 309, 106559. Retrieved 2024-11-06, from https://linkinghub.elsevier.com/retrieve/pii/S0031920119302390 doi: 10.1016/j.pepi.2020.106559
- Richardson, W. P., Stein, S., Stein, C. A., & Zuber, M. T. (1995, July). Geoid

data and thermal structure of the oceanic lithosphere. Geophysical Research Letters, 22(14), 1913-1916. Retrieved 2025-06-23, from https://agupubs.onlinelibrary.wiley.com/doi/10.1029/95GL01595 doi: 10.1029/95GL01595

- Ritsema, J., & Lekić, V. (2020, May). Heterogeneity of Seismic Wave Velocity in Earth's Mantle. Annual Review of Earth and Planetary Sciences, 48(1), 377-401. Retrieved 2025-09-02, from https://www.annualreviews.org/doi/10.1146/annurev-earth-082119-065909 doi: 10.1146/annurev-earth-082119-065909
- Ritsema, J., McNamara, A. K., & Bull, A. L. (2007, January). Tomographic filtering of geodynamic models: Implications for model interpretation and large-scale mantle structure. *Journal of Geophysical Research*, 112(B01303). Retrieved 2021-07-26, from http://doi.wiley.com/10.1029/2006JB004566 doi: 10.1029/2006JB004566
- Ritzwoller, M. H., Shapiro, N. M., & Zhong, S.-J. (2004, September). Cooling history of the Pacific lithosphere. Earth and Planetary Science Letters, 226(1-2), 69-84. Retrieved 2020-08-04, from https://linkinghub.elsevier.com/retrieve/pii/S0012821X04004662 doi: 10.1016/j.epsl.2004.07.032
- Schmeling, H., Marquart, G., & Nawa, V. (2017, May). The role of hydrothermal cooling of the oceanic lithosphere for ocean floor bathymetry and heat flow: HYDROTHERMAL COOLING OF LITHOSPHERE. Journal of Geophysical Research: Solid Earth, 122(5), 3934–3952. Retrieved 2020-08-04, from http://doi.wiley.com/10.1002/2016JB013881 doi: 10.1002/2016JB013881
- Serra, E., Zaroli, C., Lambotte, S., & Koelemeijer, P. (2025, May). Inference of the S- to P-wave velocity anomalies ratio and its uncertainty with an application to South-East Asia. California Digital Library (CDL). Retrieved 2025-07-18, from https://eartharxiv.org/repository/view/9284/ doi: 10.31223/x56x5g
- Seton, M., Müller, R. D., Zahirovic, S., Williams, S., Wright, N. M., Cannon,
 J., ... McGirr, R. (2020, October). A Global Data Set of Present-Day
 Oceanic Crustal Age and Seafloor Spreading Parameters. Geochemistry,
 Geophysics, Geosystems, 21 (10). Retrieved 2025-07-21, from https://agupubs.onlinelibrary.wiley.com/doi/10.1029/2020GC009214 (Publisher: American Geophysical Union (AGU)) doi: 10.1029/2020gc009214
- Snieder, R. (1986, March). 3-D linearized scattering of surface waves and a formalism for surface wave holography. Geophysical Journal International, 84(3), 581-605. Retrieved 2024-08-19, from https://academic.oup.com/gji/article-lookup/doi/10.1111/j.1365-246X.1986.tb04372.x doi: 10.1111/j.1365-246X.1986.tb04372.x
- Stein, C. A., & Stein, S. (1992). A model for the global variation in oceanic depth and heat flow with lithospheric age.
- team, T. p. d. (2020, February). pandas-dev/pandas: Pandas. Zenodo. Retrieved from https://doi.org/10.5281/zenodo.3509134 doi: 10.5281/zenodo.3509134
- Thrastarson, S., Van Herwaarden, D.-P., Noe, S., Josef Schiller, C., & Fichtner,
 A. (2024, June). REVEAL: A Global Full-Waveform Inversion Model. Bulletin of the Seismological Society of America, 114(3), 1392-1406. Retrieved 2025-02-18, from https://pubs.geoscienceworld.org/bssa/article/114/3/1392/637892/REVEAL-A-Global-Full-Waveform-Inversion-Model doi: 10.1785/0120230273
- Virtanen, P., Gommers, R., Oliphant, T. E., Haberland, M., Reddy, T., Cournapeau, D., ... SciPy 1.0 Contributors (2020). SciPy 1.0: Fundamental Algorithms for Scientific Computing in Python. *Nature Methods*, 17, 261–272. doi: 10.1038/s41592-019-0686-2
- Wang, Z., Singh, S. C., Prigent, C., Gregory, E. P. M., & Marjanović, M. (2022,

September). Deep hydration and lithospheric thinning at oceanic transform plate boundaries. Nature Geoscience, 15(9), 741-746. Retrieved 2025-06-26, from https://www.nature.com/articles/s41561-022-01003-3 doi: 10.1038/s41561-022-01003-3

- Wessel, P., & Haxby, W. F. (1990, January). Thermal stresses, differential subsidence, and flexure at oceanic fracture zones. *Journal of Geophysical Research:* Solid Earth, 95 (B1), 375–391. Retrieved 2025-06-23, from https://agupubs.onlinelibrary.wiley.com/doi/10.1029/JB095iB01p00375 doi: 10.1029/JB095iB01p00375
- Zaroli, C. (2016, November). Global seismic tomography using Backus-Gilbert inversion. *Geophysical Journal International*, 207(2), 876-888. Retrieved 2020-08-04, from https://academic.oup.com/gji/article-lookup/doi/10.1093/gji/ggw315 doi: 10.1093/gji/ggw315
- Zaroli, C., Koelemeijer, P., & Lambotte, S. (2017, November). Toward Seeing the Earth's Interior Through Unbiased Tomographic Lenses. Geophysical Research Letters, 44 (22), 11,399–11,408. Retrieved 2020-08-04, from https://onlinelibrary.wiley.com/doi/abs/10.1002/2017GL074996 doi: 10.1002/2017GL074996
- Zhou, Y. (2009a, March). Multimode surface wave sensitivity kernels in radially anisotropic earth media. Geophysical Journal International, 176(3), 865–888. Retrieved 2022-02-02, from https://academic.oup.com/gji/article-lookup/doi/10.1111/j.1365-246X.2008.04010.x doi: 10.1111/j.1365-246X.2008.04010.x
- Zhou, Y. (2009b, September). Surface-wave sensitivity to 3-D anelasticity. Geo-physical Journal International, 178(3), 1403-1410. Retrieved 2021-11-02, from https://academic.oup.com/gji/article-lookup/doi/10.1111/j.1365-246X.2009.04230.x doi: 10.1111/j.1365-246X.2009.04230.x
- Zhou, Y., Dahlen, F. A., & Nolet, G. (2004, July). Three-dimensional sensitivity kernels for surface wave observables. Geophysical Journal International, 158(1), 142–168. Retrieved 2020-08-04, from https://academic.oup.com/gji/article-lookup/doi/10.1111/j.1365-246X.2004.02324.x doi: 10.1111/j.1365-246X.2004.02324.x
- Zhou, Y., Nolet, G., Dahlen, F. A., & Laske, G. (2006). Global upper-mantle structure from finite-frequency surface-wave tomography. *Journal of Geophysical Research*, 111 (B04304). Retrieved 2020-08-04, from http://doi.wiley.com/10.1029/2005JB003677 doi: 10.1029/2005JB003677

Supporting information for: New insights into the cooling of the oceanic lithosphere from surface-wave tomographic inferences

Franck Latallerie¹, Paula Koelemeijer¹, Andrew Walker¹, Alessia Maggi², Sophie Lambotte², Christophe Zaroli²

¹Department of Earth Sciences, University of Oxford, Oxford, United Kingdom
 ²Institut Terre et Environement de Strasbourg, UMR7063, Université de Strasbourg, EOST/CNRS,
 67084, Strasbourg, France

Supporting information

This supporting information file contains Table 1, Figures 1 to 5, and references to seismic networks.

Tables and figures

Table 1. Details of tomography models shown in Figure 5 and Figure 1

Name	Forward	Inverse	Parameters	Parameterisation	Data	Domain
SS3DPacific	Born FF	SOLA 3D	Vsv	Local	R fund. phase	Uppermost-mantle
SS2DPacific	Ray	Data-misfit + SOLA 2D	Vsv	Local	R multi. phase	Upper-mantle
FFSW1	Born FF	Data-misfit	Vsv, Vsh	Local	R/G fund. phase	Upper-mantle
REVEAL	Adjoint	Data-misfit	Vsv, Vsh, Vp	Local	Full-waveform	Whole-mantle
GLAD-M35	Adjoint	Data-misfit	Vsv, Vsh, Vp, eta	Local	Full-waveform	Whole-mantle
SEMUCB-WM1	SEM-NACT	Data-misfit	Vs, Vsh/Vsv	Local	Full-waveform	Whole-mantle
SGLOBE-RANI	Ray	Data-misfit	Vs, $\frac{Vsh^2 - Vsv^2}{2Vs^2}$, ρ	Global	R/G multi. phase/group, TT	Whole-mantle
S362ANI	Ray	Data-misfit	Vs, Vsh-Vsv, Vph-Vpv	Global	R/G fund. phase, body waveform, TT	Whole-mantle

 $FF: Finite-frequency, R: Rayleigh, G: Love, fund.: fundamental, multi.: multimode, TT: Body-wave traveltimes, <math>\rho: density.$

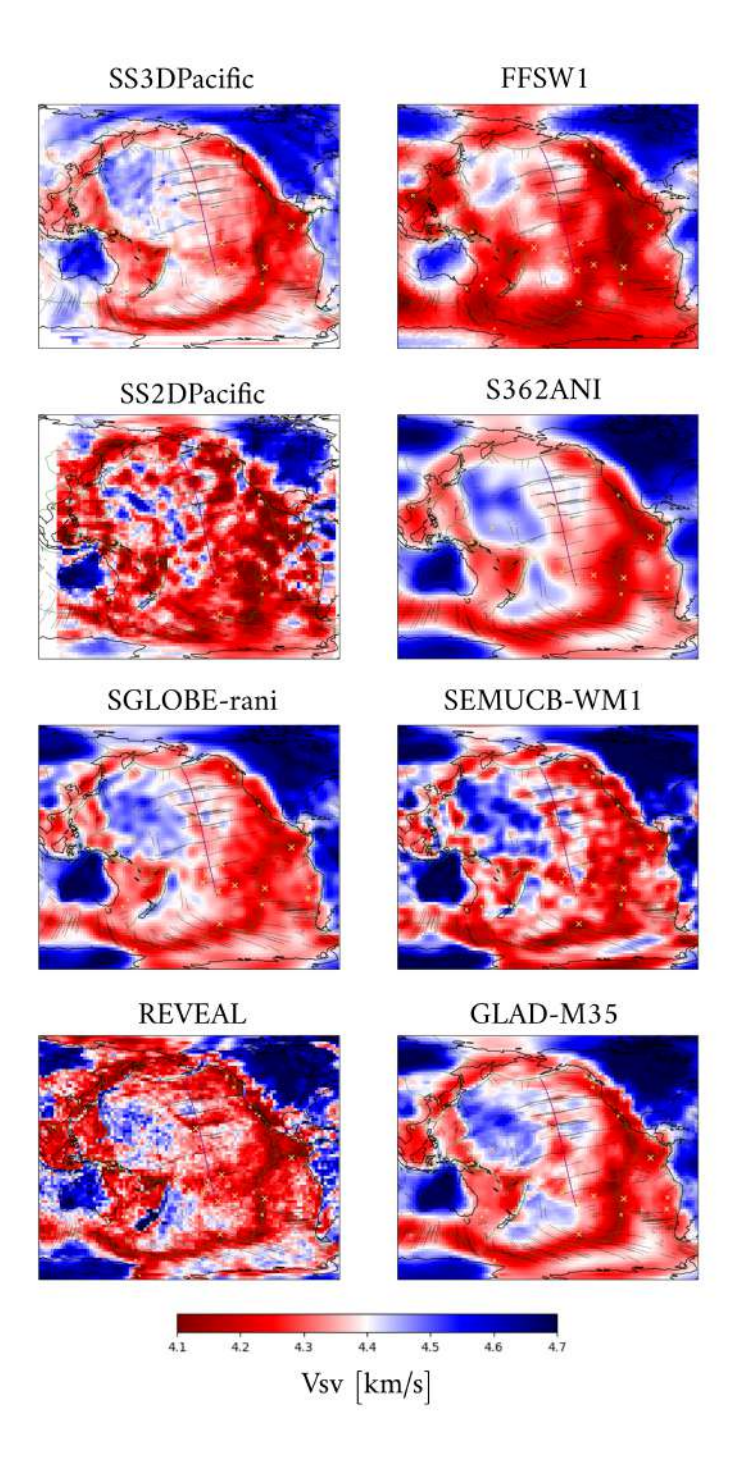


Figure 1. Comparison of the absolute Vsv structure of SS3DPacific compared to a selection of tomography models at 112 km depth. We include SS2DPacific (Latallerie et al., 2022),

- SGLOBE-rani (Chang et al., 2015), REVEAL:(Thrastarson et al., 2024), FFSW1 (Zhou et al.,
- $_{5}$ $\,$ 2006), S362ANI (Kustowski et al., 2008), SEMUCB-WM1 (French & Romanowicz, 2014), and
- 6 GLAD-M35 (Cui et al., 2024).

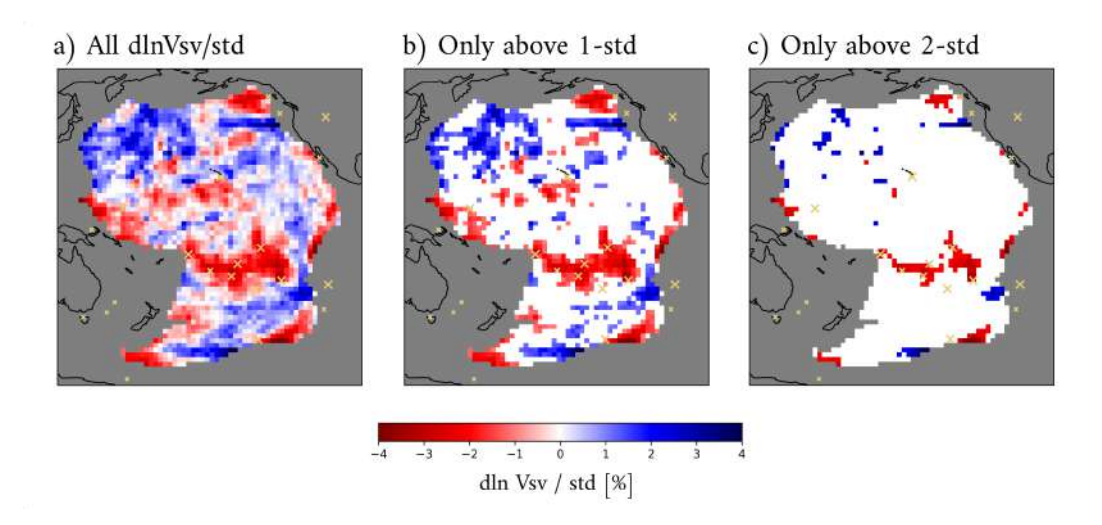


Figure 2. Significant lateral features in SS3DPacific, obtained by removing the agedependence trend and normalising by the model uncertainty (std). We include a) all features,
or mask values below b) the 1-σ or c) the 2-σ level. Yellow crosses indicate hotspot locations, see
the caption of Figure 1 in the main text.

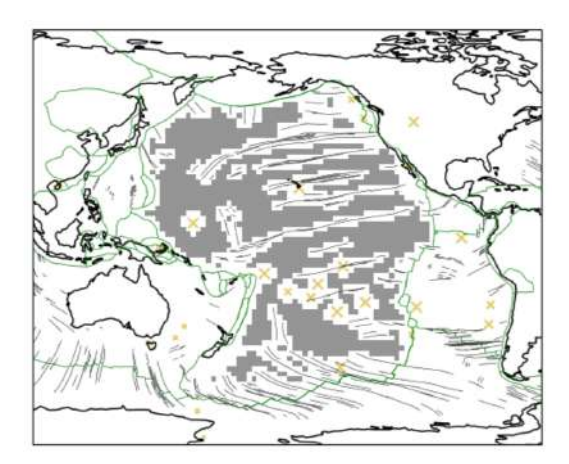


Figure 3. Mask used to calculate the trends of the average velocity with age. Grey cells indicate regions that are included, while regions near hotspots (yellow crosses), fracture zones (black lines), and plate boundaries (green lines) are excluded. See the caption of Figure 1 in the main text for more details.

11

12

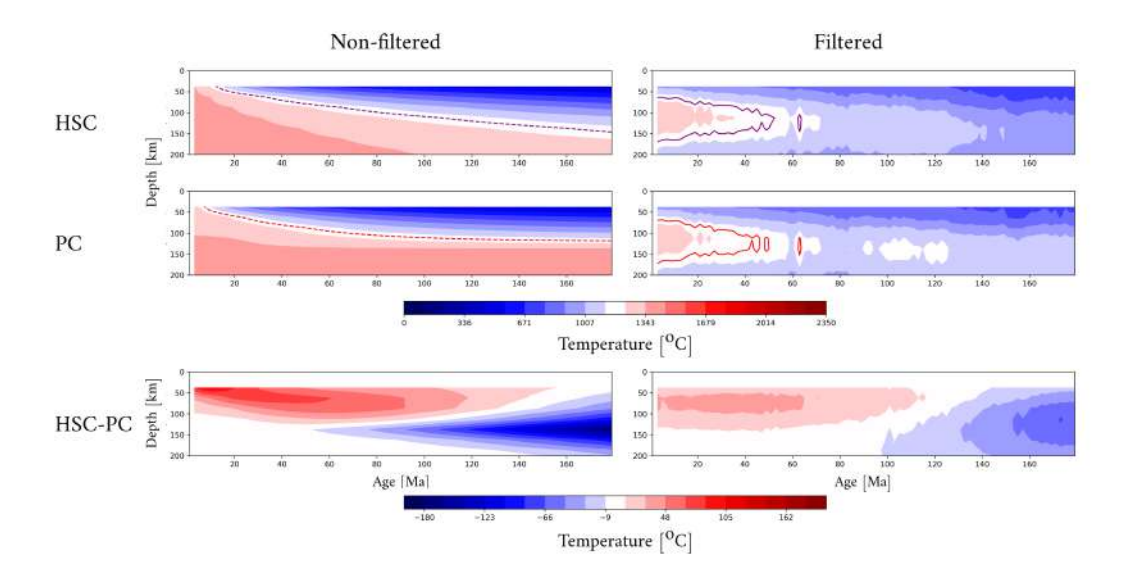


Figure 4. Thermal structure according to models HSC (first row) and PC (second row), as well as their differences (last row). The left column shows the original, non-filtered thermal structure and the second column shows the filtered version using the SS3DPacific tomographic filter.

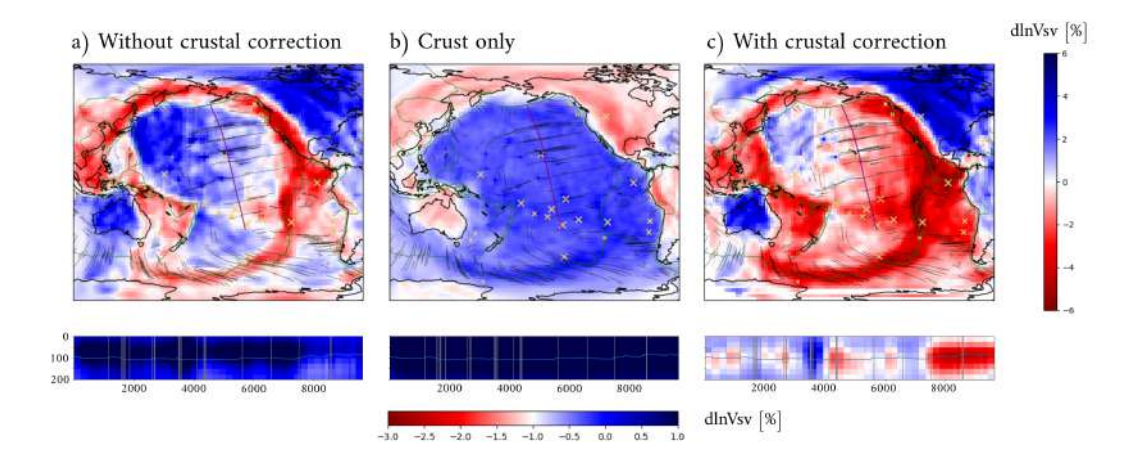


Figure 5. Assessment of influence of crustal structure on the model solution, showing results for SOLA inference of a) data without crustal corrections applied, b) only predictions for crustal structure, and c) data with crustal corrections (i.e. SS3DPacific). We use a different colorscale for the cross-sections to better represent the range of velocities shown.

Citations for seismic networks used in this study

We list here the network codes (in bold) for stations analysed in this study followed by the full citation as per the FDSN website, where available.

- IP: Anya Reading and Nick Rawlinson (2011); Ritter et al. (2014); Douglas Wiens and Maria Beatrice Magnani (2018); Sarah Mader et al. (2022)
- **6E** James Conder (2013); John Louie (2018); Pieter-Ewald Share and Frank Vernon (2019); Elnaz Seylabi et al. (2021); Dahm et al. (2023); Susan Bilek (2024)
- 7A Ryberg and Haberland (2008); Ramon Carbonell (2012); Maureen Long and Paul Wiita (2013); Nicholas Schmerr (2017); Christopher W Johnson et al. (2018); Yuan et al. (2019); Marcelo Rocha (2021); Neil Harbison and Craig O'Neill (2024)
- 7C Vergne et al. (2014); Rufus Catchings (2014); Derek Schutt and Rick Aster (2015); Costanzo et al. (2022)
- **7D** Brian Kennett (1997); Wes Thelen and Paul Bodin (2009); IRIS OBSIP (2011); Wenyuan Fan et al. (2018); Calum Chamberlain (2022)
- **AE** Arizona Geological Survey (2007)
- AI Istituto Nazionale di Oceanografia e di Geofisica Sperimentale (1992)
- AK Alaska Earthquake Center, Univ. of Alaska Fairbanks (1987)
- AR No DOI
- AT NOAA National Oceanic and Atmospheric Administration (USA) (1967)
- AU Geoscience Australia (2021)
- AV Alaska Volcano Observatory-USGS (1988)
- AZ Frank Vernon (1982)
- BK Northern California Earthquake Data Center (2014)
- C No DOI
- C1 Universidad de Chile (2012)
- CB Institute of Geophysics China Earthquake Administration (IGPCEA) (2000)
- CC Cascades Volcano Observatory/USGS (2001)
- CI California Institute of Technology and United States Geological Survey Pasadena (1926)
- CM Servicio Geológico Colombiano (1993)
- CN Natural Resources Canada (1975)
- CU Albuquerque Seismological Laboratory (ASL)/USGS (2006)
- DK GEUS Geological Survey of Denmark and Greenland (1976)
- G Institut de physique du globe de Paris (IPGP) and École et Observatoire des Sciences de la Terre de Strasbourg (EOST) (1982)
- **GG** IRIS HQ (DC) (2012)
- GS Albuquerque Seismological Laboratory (ASL)/USGS (1980)
- GT Albuquerque Seismological Laboratory (ASL)/USGS (1993)
- IC Albuquerque Seismological Laboratory (ASL)/USGS (1992)
- II Scripps Institution of Oceanography (1986)
- IM Various Institutions (1965)
- IU Albuquerque Seismological Laboratory/USGS (1988)
- JP No DOI
- KS No DOI
- LB No DOI
- LD Lamont Doherty Earth Observatory (LDEO), Columbia University (1970)
- MI USGS Alaska Anchorage (2000)
- MM Department of Meteorology and Hydrology National Earthquake Data Center (2016)

- MX Servicio Sismológico Nacional, Instituto de Geofísica, Universidad Nacional Autónoma de México, México (2017)
- MY No DOI
- N4 Albuquerque Seismological Laboratory/USGS (2013)
- NA KNMI (2006)
- NE Albuquerque Seismological Laboratory (ASL)/USGS (1994)
- NM No DOI
- NN University of Nevada, Reno (1971)
- NR Utrecht University (UU Netherlands) (1983)
- NU Instituto Nicaraguense de Estudios Territoriales (INETER) (1975)
- OO NSF Ocean Observatories Initiative (2013)
- PB No DOI
- PE Penn State University (2004)
- PN No DOI
- PR University of Puerto Rico (1986)
- PS No DOI
- PY Frank Vernon (2014)
- RM Regional Integrated Multi-Hazard Early Warning System (RIMES Thailand) (2008)
- RV Alberta Geological Survey / Alberta Energy Regulator (2013)
- $\mathbf{S1}$ Michelle Salmon et al. (2011)
- SC New Mexico Tech (1999)
- SV No DOI
- TA IRIS Transportable Array (2003)
- TM No DOI
- TW Institute of Earth Sciences, Academia Sinica, Taiwan (1996)
- TX Bureau of Economic Geology, The University of Texas at Austin (2016)
- **UO** University of Oregon (1990)
- US Albuquerque Seismological Laboratory (ASL)/USGS (1990)
- UW University of Washington (1963)
- WI Institut De Physique Du Globe De Paris (IPGP) (2008)
- XF Frank Vernon and Jon Fletcher (1987); Steve Day and Frank Vernon (1994); Sridhar Anandakrishnan (1995); Frank Vernon and Ken Dueker (2000); John Nabelek (2002); Steve Grand and Jim Ni (2006); Chris Larsen and Michael West (2009); Douglas Wiens (2012); Meredith Nettles (2014); S. De Angelis and A. Diaz-Moreno (2017); Tiberi et al. (2020); Haberland et al. (2021); Anne Meltzer et al. (2021); Pilz et al. (2023); Paul et al. (2024)
- XZ Rick Aster and Philip Kyle (1999); Anthony Qamar (2001); Sylvie Leroy (2003); Roger Hansen and Gary Pavlis (2005); Chris Hayward (2014); Christian Poppeliers (2015); Frank Kruger et al. (2016); Silvio De Angelis (2018); Andy Nyblade (2019); SOCQUET et al. (2020)
- Y6 Ian Joughin et al. (2006); Keir et al. (2016); Jamie Farrell et al. (2018); John Louie and Ronald Breitmeyer (2019); Tilmann et al. (2021); Weisen Shen (2023)
- YP Steve Grand and Jim Ni (2009); Zhao et al. (2016); Cornou et al. (2014); Gordon Hamilton (2016); Doubre et al. (2021); Amanda Bustin (2019)
- **Z7** Dan Klinglesmith (2008); Robert White (2010); Paul Bedrosian et al. (2017); Vergne and RESIF (2021); Tulane University et al. (2019); Dietrich Lange and Marcos Moreno (2023); Noah Finnegan and Susan Schwartz (2023)

References

- Alaska Earthquake Center, Univ. of Alaska Fairbanks. (1987). Alaska geophysical network. International Federation of Digital Seismograph Networks. Retrieved from https://www.fdsn.org/networks/detail/AK/ doi: 10.7914/SN/AK
- Alaska Volcano Observatory-USGS. (1988). Alaska volcano observatory. International Federation of Digital Seismograph Networks. Retrieved from https://www.fdsn.org/networks/detail/AV/doi: 10.7914/SN/AV
- Alberta Geological Survey / Alberta Energy Regulator. (2013). Regional alberta observatory for earthquake studies network. International Federation of Digital Seismograph Networks. Retrieved from https://www.fdsn.org/networks/detail/RV/doi: 10.7914/SN/RV
- Albuquerque Seismological Laboratory (ASL)/USGS. (1980). Us geological survey networks. International Federation of Digital Seismograph Networks. Retrieved from https://www.fdsn.org/networks/detail/GS/ doi: 10.7914/SN/GS
- Albuquerque Seismological Laboratory (ASL)/USGS. (1990). United states national seismic network. International Federation of Digital Seismograph Networks. Retrieved from https://www.fdsn.org/networks/detail/US/ doi: 10.7914/SN/US
- Albuquerque Seismological Laboratory (ASL)/USGS. (1992). New china digital seismograph network. International Federation of Digital Seismograph Networks. Retrieved from https://www.fdsn.org/networks/detail/IC/ doi: 10.7914/SN/IC
- Albuquerque Seismological Laboratory (ASL)/USGS. (1993). Global telemetered seismograph network (usaf/usgs). International Federation of Digital Seismograph Networks. Retrieved from https://www.fdsn.org/networks/detail/GT/doi: 10.7914/SN/GT
- Albuquerque Seismological Laboratory (ASL)/USGS. (1994). New england seismic network. International Federation of Digital Seismograph Networks. Retrieved from https://www.fdsn.org/networks/detail/NE/ doi: 10.7914/SN/NE
- Albuquerque Seismological Laboratory (ASL)/USGS. (2006). Caribbean network. International Federation of Digital Seismograph Networks. Retrieved from https://www.fdsn.org/networks/detail/CU/doi: 10.7914/SN/CU
- Albuquerque Seismological Laboratory/USGS. (1988). Global seismograph network (gsn iris/usgs). International Federation of Digital Seismograph Networks. Retrieved from https://www.fdsn.org/networks/detail/IU/ doi: 10.7914/SN/IU
- Albuquerque Seismological Laboratory/USGS. (2013). Central and eastern us network. International Federation of Digital Seismograph Networks. Retrieved from https://www.fdsn.org/networks/detail/N4/doi: 10.7914/SN/N4
- Amanda Bustin. (2019). *Ubcism*. International Federation of Digital Seismograph Networks. Retrieved from https://www.fdsn.org/networks/detail/YP_2019/doi: 10.7914/SN/YP_2019
- Andy Nyblade. (2019). Shale hills critical zone observatory mini-array experiment. International Federation of Digital Seismograph Networks. Retrieved from https://www.fdsn.org/networks/detail/XZ_2019/ doi: 10.7914/SN/XZ_2019
- Anne Meltzer, Susan Beck, & Joshua Stachnik. (2021). High resolution imaging of the pedernales earthquake rupture zone broadbands. International Federation of Digital Seismograph Networks. Retrieved from https://www.fdsn.org/networks/detail/XF_2021/ doi: 10.7914/SN/XF_2021
- Anthony Qamar. (2001). Spokane wa earthquake swarm. International Federation of Digital Seismograph Networks. Retrieved from https://www.fdsn.org/networks/detail/XZ_2001/ doi: 10.7914/SN/XZ_2001
- Anya Reading, & Nick Rawlinson. (2011). Bass strait. International Federation of Digital Seismograph Networks. Retrieved from https://www.fdsn.org/

- networks/detail/1P_2011/ doi: $10.7914/SN/1P_2011$
- Arizona Geological Survey. (2007). Arizona broadband seismic network. International Federation of Digital Seismograph Networks. Retrieved from https://www.fdsn.org/networks/detail/AE/ doi: 10.7914/SN/AE
- Brian Kennett. (1997). Kimba97. International Federation of Digital Seismograph Networks. Retrieved from https://www.fdsn.org/networks/detail/7D_1997/ doi: 10.7914/SN/7D_1997
- Bureau of Economic Geology, The University of Texas at Austin. (2016). Texas seismological network. International Federation of Digital Seismograph Networks. Retrieved from https://www.fdsn.org/networks/detail/TX/ doi: 10.7914/SN/TX
- California Institute of Technology and United States Geological Survey Pasadena. (1926). Southern california seismic network. International Federation of Digital Seismograph Networks. Retrieved from https://www.fdsn.org/networks/detail/CI/doi: 10.7914/SN/CI
- Calum Chamberlain. (2022). Puysegur tremor and nucleation geophysical observatory. International Federation of Digital Seismograph Networks. Retrieved from https://www.fdsn.org/networks/detail/7D_2022/ doi: 10.7914/SN/7D_2022
- Cascades Volcano Observatory/USGS. (2001). Cascade chain volcano monitoring. International Federation of Digital Seismograph Networks. Retrieved from https://www.fdsn.org/networks/detail/CC/doi: 10.7914/SN/CC
- Chang, S.-J., Ferreira, A. M. G., Ritsema, J., van Heijst, H. J., & Woodhouse, J. H. (2015, June). Joint inversion for global isotropic and radially anisotropic mantle structure including crustal thickness perturbations: RADIALLY ANISOTROPIC MANTLE STRUCTURE. Journal of Geophysical Research: Solid Earth, 120(6), 4278–4300. Retrieved 2023-02-06, from http://doi.wiley.com/10.1002/2014JB011824 doi: 10.1002/2014JB011824
- Chris Hayward. (2014). *Idaho teton dam*. International Federation of Digital Seismograph Networks. Retrieved from https://www.fdsn.org/networks/detail/XZ_2014/ doi: 10.7914/SN/XZ_2014
- Chris Larsen, & Michael West. (2009). Collaborative research: Relating glaciergenerated seismicity to ice motion, basal processes and iceberg calving. International Federation of Digital Seismograph Networks. Retrieved from https:// www.fdsn.org/networks/detail/XF_2009/ doi: 10.7914/SN/XF_2009
- Christian Poppeliers. (2015). Measuring ambient noise of ocean breakers. International Federation of Digital Seismograph Networks. Retrieved from https://www.fdsn.org/networks/detail/XZ_2015/ doi: 10.7914/SN/XZ_2015
- Christopher W Johnson, Frank Vernon, Yehuda Ben-Zion, & Norimitsu Nakata. (2018). Sage brush flats seismic experiment on interaction of wind with ground motion. International Federation of Digital Seismograph Networks. Retrieved from https://www.fdsn.org/networks/detail/7A_2018/ doi: 10.7914/SN/7A_2018
- Cornou, C., Bard, P.-Y., & RESIF. (2014). Seismic network yp:french part of the argostoli (greece) aftershock experiment (resif-sismob). RESIF Réseau Sismologique et géodésique Français. Retrieved from https://seismology.resif.fr/networks/\#/YP_2014 doi: 10.15778/RESIF.YP2014
- Costanzo, A., Falcone, S., La Piana, C., Caserta, A., Doumaz, F., Buongiorno, M. F., ... Speciale, S. (2022, April). *Urban Seismic Network (RUSN-CAL-INGV) Real time Urban Seismic Network managed by CALabrian headquar-ters of INGV for monitoring urban areas, critical infrastructures and cultural heritage sites*. Istituto Nazionale di Geofisica e Vulcanologia (INGV). Retrieved from https://eida.ingv.it/en/network/7C_2021 (Artwork Size: 1 GB per day Pages: 1 GB per day) doi: 10.13127/SD/O5NRHMP9N7
- Cui, C., Lei, W., Liu, Q., Peter, D., Bozdağ, E., Tromp, J., ... Pugmire, D. (2024,

- August). GLAD-M35: a joint P and S global tomographic model with uncertainty quantification. Geophysical Journal International, 239(1), 478–502. Retrieved 2025-07-18, from https://academic.oup.com/gji/article/239/1/478/7727823 (Publisher: Oxford University Press (OUP)) doi: 10.1093/gji/ggae270
- Dahm, T., Isken, M. P., Milkereit, C., Mikulla, S., Yuan, X., Sens-Schönfelder, C., ... Busch, S. (2023). *Eifel large-n seismic network (elsn)*. GFZ Data Services. Retrieved from https://geofon.gfz-potsdam.de/doi/network/6E/2022 doi: 10.14470/1R080930
- Dan Klinglesmith. (2008). Mroi vibration studies. International Federation of Digital Seismograph Networks. Retrieved from https://www.fdsn.org/networks/detail/Z7_2008/ doi: 10.7914/SN/Z7_2008
- Department of Meteorology and Hydrology National Earthquake Data Center. (2016). Myanmar national seismic network. International Federation of Digital Seismograph Networks. Retrieved from https://www.fdsn.org/networks/detail/MM/doi: 10.7914/SN/MM
- Derek Schutt, & Rick Aster. (2015). The mackenzie mountains transect: Active deformation from margin to craton. International Federation of Digital Seismograph Networks. Retrieved from https://www.fdsn.org/networks/detail/7C_2015/ doi: 10.7914/SN/7C_2015
- Dietrich Lange, & Marcos Moreno. (2023). So297-land: Onshore extension of the 2023 rv so297 eperiment between copiapó and taltal, chile. International Federation of Digital Seismograph Networks. Retrieved from https://www.fdsn.org/networks/detail/Z7_2023/ doi: 10.7914/KHGA-FW51
- Doubre, C., Leroy, S., Keir, D., Pagli, C., & RESIF. (2021). Study of the structure of the lithosphere from the continental plateau of western ethiopia to the active afar rift (resif-sismob). RESIF Réseau Sismologique et géodésique Français. Retrieved from https://seismology.resif.fr/networks/\#/YP__2017 doi: 10.15778/RESIF.YP2017
- Douglas Wiens. (2012). Mantle serpentinization and water cycling through the mariana trench and forearc. International Federation of Digital Seismograph Networks. Retrieved from https://www.fdsn.org/networks/detail/XF_2012/doi: 10.7914/SN/XF_2012
- Douglas Wiens, & Maria Beatrice Magnani. (2018). Solid earth response of the patagonia andes to post-little ice age glacial retreat. International Federation of Digital Seismograph Networks. Retrieved from https://www.fdsn.org/networks/detail/1P_2018/ doi: 10.7914/SN/1P_2018
- Elnaz Seylabi, Scott Tyler, Rachel Hatch, & Seth Saltiel. (2021). Sub-surface imaging of the west reno basin. International Federation of Digital Seismograph Networks. Retrieved from https://www.fdsn.org/networks/detail/6E_2021/ doi: 10.7914/SN/6E_2021
- Frank Kruger, Andreas Rietbrock, Catherine Rychert, Nicholas Harmon, & Jenny Collier. (2016). Volatile recycling at the lesser antilles arc: Processes and consequences. International Federation of Digital Seismograph Networks. Retrieved from https://www.fdsn.org/networks/detail/XZ_2016/ doi: 10.7914/SN/XZ_2016
- Frank Vernon. (1982). Anza regional network. International Federation of Digital Seismograph Networks. Retrieved from https://www.fdsn.org/networks/detail/AZ/doi: 10.7914/SN/AZ
- Frank Vernon. (2014). Piñon flats observatory array. International Federation of Digital Seismograph Networks. Retrieved from https://www.fdsn.org/networks/detail/PY/doi: 10.7914/SN/PY
- Frank Vernon, & Jon Fletcher. (1987). Anza borehole experiment. International Federation of Digital Seismograph Networks. Retrieved from https://www.fdsn.org/networks/detail/XF_1987/ doi: 10.7914/SN/XF_1987

- Frank Vernon, & Ken Dueker. (2000). Laramie telemetered broad-band array. International Federation of Digital Seismograph Networks. Retrieved from https://www.fdsn.org/networks/detail/XF_2000/ doi: $10.7914/SN/XF_2000$
- French, S. W., & Romanowicz, B. A. (2014, December). Whole-mantle radially anisotropic shear velocity structure from spectral-element waveform tomography. Geophysical Journal International, 199(3), 1303–1327. Retrieved 2022-10-09, from http://academic.oup.com/gji/article/199/3/1303/612270/Wholemantle-radially-anisotropic-shear-velocity doi: 10.1093/gji/ggu334
- Geoscience Australia. (2021). Australian national seismograph network data collection. Commonwealth of Australia (Geoscience Australia). Retrieved from http://pid.geoscience.gov.au/dataset/ga/144675 doi: 10.26186/144675
- GEUS Geological Survey of Denmark and Greenland. (1976). Danish seismological network. International Federation of Digital Seismograph Networks. Retrieved from https://www.fdsn.org/networks/detail/DK/doi: 10.7914/NW3X-DF02
- Gordon Hamilton. (2016). Flow and fracture dynamics in an ice shelf lateral margin: Observations and modeling of the mcmurdo shear zone. International Federation of Digital Seismograph Networks. Retrieved from https://www.fdsn.org/networks/detail/YP_2016/ doi: 10.7914/SN/YP_2016
- Haberland, C., Ryberg, T., & Kirsch, M. (2021). The geyer seismic network. GFZ Data Services. Retrieved from https://geofon.gfz-potsdam.de/doi/network/XF/2020 doi: 10.14470/KS7575632014
- Ian Joughin, Sarah Das, & Mark Behn. (2006). Behavior of supraglacial lakes and their role in outlet glacier dynamics and mass balance of the greenland ice sheet. International Federation of Digital Seismograph Networks. Retrieved from https://www.fdsn.org/networks/detail/Y6_2006/ doi: 10.7914/SN/Y6_2006
- Institut De Physique Du Globe De Paris (IPGP). (2008). Gnss, seismic broadband and strong motion permanent networks in west indies. Institut de physique du globe de Paris (IPGP), Université de Paris. Retrieved from http://volobsis.ipgp.fr/networks/detail/WI/doi: 10.18715/ANTILLES.WI
- Institut de physique du globe de Paris (IPGP), & École et Observatoire des Sciences de la Terre de Strasbourg (EOST). (1982). Geoscope, french global network of broad band seismic stations. Institut de physique du globe de Paris (IPGP), Université de Paris. Retrieved from http://geoscope.ipgp.fr/networks/detail/G/ doi: 10.18715/GEOSCOPE.G
- Institute of Earth Sciences, Academia Sinica, Taiwan. (1996). Broadband array in taiwan for seismology. International Federation of Digital Seismograph Networks. Retrieved from https://www.fdsn.org/networks/detail/TW/ doi: 10.7914/SN/TW
- Institute of Geophysics China Earthquake Administration (IGPCEA). (2000). China national seismic network, data management centre of china national seismic network at institute of geophysics, cea. International Federation of Digital Seismograph Networks. Retrieved from https://www.fdsn.org/networks/detail/CB/doi: 10.7914/SN/CB
- Instituto Nicaraguense de Estudios Territoriales (INETER). (1975). Nicaraguan seismic network. International Federation of Digital Seismograph Networks. Retrieved from https://www.fdsn.org/networks/detail/NU/doi: 10.7914/SN/NU
- IRIS HQ (DC). (2012). Greenland ice sheet monitoring network. International Federation of Digital Seismograph Networks. Retrieved from https://www.fdsn.org/networks/detail/GG/doi: 10.7914/SN/GG

- IRIS OBSIP. (2011). Cascadia initiative community experiment obs component. International Federation of Digital Seismograph Networks. Retrieved from https://www.fdsn.org/networks/detail/7D_2011/ doi: 10.7914/SN/7D_2011
- IRIS Transportable Array. (2003). Usarray transportable array. International Federation of Digital Seismograph Networks. Retrieved from https://www.fdsn.org/networks/detail/TA/ doi: 10.7914/SN/TA
- Istituto Nazionale di Oceanografia e di Geofisica Sperimentale. (1992). Antarctic seismographic argentinean italian network asain. International Federation of Digital Seismograph Networks. Retrieved from https://www.fdsn.org/networks/detail/AI/ doi: 10.7914/SN/AI
- James Conder. (2013). Wabash valley seismic zone. International Federation of Digital Seismograph Networks. Retrieved from https://www.fdsn.org/networks/detail/6E_2013/ doi: 10.7914/SN/6E_2013
- Jamie Farrell, Keith Koper, & Robert Sohn. (2018). Yellowstone lake microseism 2018. International Federation of Digital Seismograph Networks. Retrieved from https://www.fdsn.org/networks/detail/Y6_2018/ doi: 10.7914/SN/Y6_2018
- John Louie. (2018). Surface-wave characterization of the shoal nuclear blast cavity and rubble chimney. International Federation of Digital Seismograph Networks. Retrieved from https://www.fdsn.org/networks-detail/6E_2018/ doi: 10.7914/SN/6E_2018
- John Louie, & Ronald Breitmeyer. (2019). Community, arts, and environmental setting of fly geyser, nevada. International Federation of Digital Seismograph Networks. Retrieved from https://www.fdsn.org/networks/detail/Y6_2019/ doi: 10.7914/SN/Y6_2019
- John Nabelek. (2002). Collaborative research: Lithospheric scale dynamics of active mountain building along the himalayan-tibetan collision zone. International Federation of Digital Seismograph Networks. Retrieved from https://www.fdsn.org/networks/detail/XF_2002/ doi: 10.7914/SN/XF_2002
- Keir, Kendall, & Ayele. (2016). Rift valley volcanism past present and future. International Federation of Digital Seismograph Networks. Retrieved from https://www.fdsn.org/networks/detail/Y6_2016/ doi: 10.7914/SN/Y6_2016
- KNMI. (2006). Caribbean netherlands seismic network. Royal Netherlands Meteorological Institute (KNMI). Retrieved from http://rdsa.knmi.nl/network/NA/doi: 10.21944/DFFA7A3F-7E3A-3B33-A436-516A01B6AF3F
- Kustowski, B., Ekström, G., & Dziewoński, A. M. (2008, June). Anisotropic shearwave velocity structure of the Earth's mantle: A global model. *Journal of Geophysical Research*, 113(B6), B06306. Retrieved 2022-10-03, from http://doi.wiley.com/10.1029/2007JB005169 doi: 10.1029/2007JB005169
- Lamont Doherty Earth Observatory (LDEO), Columbia University. (1970). Lamont-doherty cooperative seismographic network. International Federation of Digital Seismograph Networks. Retrieved from https://www.fdsn.org/networks/detail/LD/doi: 10.7914/SN/LD
- Latallerie, F., Zaroli, C., Lambotte, S., & Maggi, A. (2022, April). Analysis of tomographic models using resolution and uncertainties: a surface wave example from the Pacific. *Geophysical Journal International*, 230(2), 893-907. Retrieved 2022-04-20, from https://academic.oup.com/gji/article/230/2/893/6544670 doi: 10.1093/gji/ggac095
- Marcelo Rocha. (2021). Carajás mineral province seismic network. International Federation of Digital Seismograph Networks. Retrieved from https://www.fdsn.org/networks/detail/7A_2021/ doi: 10.7914/SN/7A_2021
- Maureen Long, & Paul Wiita. (2013). *Mid-atlantic geophysical integrative collabo*ration. International Federation of Digital Seismograph Networks. Retrieved

- from https://www.fdsn.org/networks/detail/7A_2013/ doi: $10.7914/SN/7A_2013$
- Meredith Nettles. (2014). Understanding precambrian to present assembly of greenland. International Federation of Digital Seismograph Networks. Retrieved from https://www.fdsn.org/networks/detail/XF_2014/ doi: 10.7914/SN/XF_2014
- Michelle Salmon, Natalie Balfour, Malcolm Sambridge, Sima Mousavi, & Robert Pickle. (2011). Australian seismometers in schools. AusPass. Retrieved from https://www.fdsn.org/networks/detail/S1/doi: 10.7914/SN/S1
- Natural Resources Canada. (1975). Canadian national seismograph network. Natural Resources Canada. Retrieved from https://www.fdsn.org/networks/detail/CN/doi: 10.7914/SN/CN
- Neil Harbison, & Craig O'Neill. (2024). Georgetown seismic traverse, north queensland. International Federation of Digital Seismograph Networks. Retrieved from https://www.fdsn.org/networks/detail/7A_2024/ doi: 10.7914/3V05-SW22
- New Mexico Tech. (1999). New mexico tech seismic network. International Federation of Digital Seismograph Networks. Retrieved from https://www.fdsn.org/networks/detail/SC/doi: 10.7914/0ABK-1345
- Nicholas Schmerr. (2017). Geodes san francisco volcanic field active seismic experiment 2017. International Federation of Digital Seismograph Networks. Retrieved from https://www.fdsn.org/networks/detail/7A_2017/ doi: 10.7914/TYZX-JN40
- NOAA National Oceanic and Atmospheric Administration (USA). (1967). National tsunami warning center alaska seismic network. International Federation of Digital Seismograph Networks. Retrieved from https://www.fdsn.org/networks/detail/AT/ doi: 10.7914/SN/AT
- Noah Finnegan, & Susan Schwartz. (2023). Nodal seismometer deployment at oak ridge earthflow near san jose, ca. International Federation of Digital Seismograph Networks. Retrieved from https://www.fdsn.org/networks/detail/Z7_2023/ doi: 10.7914/PNFW-J315
- Northern California Earthquake Data Center. (2014). Berkeley digital seismic network (bdsn). Northern California Earthquake Data Center. Retrieved from https://ncedc.org/bk_doi_metadata.html doi: 10.7932/BDSN
- NSF Ocean Observatories Initiative. (2013). Ocean observatories initiative. International Federation of Digital Seismograph Networks. Retrieved from https://www.fdsn.org/networks/detail/00/doi: 10.7914/SN/OO
- Paul, A., Mordret, A., Aubert, C., Chevrot, S., Sylvander, M., Pauchet, H., & RESIF. (2024). Maciv-profiles temporary experiment of seismic imaging of the lithospheric structure of the french massif central along 3 profiles to complete the maciv-bb broadband network to be deployed in 2024, france (resif-sismob). RESIF Réseau Sismologique et géodésique Français. Retrieved from https://seismology.resif.fr/networks/\#/XF_2024 doi: 10.15778/RESIF.XF2024
- Paul Bedrosian, Jake R Morris, Margaret Goldman, & Benjamin R. Bloss. (2017). Kansas and nebraska magnetotelluric time series (usgs-gggsc, kansas 2017 long period). International Federation of Digital Seismograph Networks. Retrieved from https://www.fdsn.org/networks/detail/Z7_2017/ doi: 10.7914/SN/Z7_2017
- Penn State University. (2004). Pennsylvania state seismic network. International Federation of Digital Seismograph Networks. Retrieved from https://www.fdsn.org/networks/detail/PE/ doi: 10.7914/SN/PE
- Pieter-Ewald Share, & Frank Vernon. (2019). Dense nodal deployment at some test sites for the upcoming faultscan project. International Federation of Digital Seismograph Networks. Retrieved from https://www.fdsn.org/networks/

- $detail/6E_2019/doi: 10.7914/SN/6E_2019$
- Pilz, M., Ohrnberger, M., & Roux, P. (2023). *Meta-wt.* GFZ Data Services. Retrieved from https://geofon.gfz-potsdam.de/doi/network/XF/2023 doi: 10.14470/KS178126
- Ramon Carbonell. (2012). Wide-angle seismic reflection experiment across the central iberian zone; iberia peninsula. International Federation of Digital Seismograph Networks. Retrieved from https://www.fdsn.org/networks/detail/7A_2012/ doi: 10.7914/SN/7A_2012
- Regional Integrated Multi-Hazard Early Warning System (RIMES Thailand). (2008). Regional integrated multi-hazard early warning system. International Federation of Digital Seismograph Networks. Retrieved from https://www.fdsn.org/networks/detail/RM/doi: 10.7914/SN/RM
- Rick Aster, & Philip Kyle. (1999). Mount erebus seismic studies. International Federation of Digital Seismograph Networks. Retrieved from https://www.fdsn.org/networks/detail/XZ_1999/ doi: 10.7914/SN/XZ_1999
- Ritter, J. R. R., Schmidt, B., Haberland, C., & Weber, M. (2014). Deep-tee phase 1. GFZ Data Services. Retrieved from https://geofon.gfz-potsdam.de/doi/network/1P/2014 doi: 10.14470/6C709520
- Robert White. (2010). Northern volcanic zone. International Federation of Digital Seismograph Networks. Retrieved from https://www.fdsn.org/networks/detail/Z7_2010/ doi: 10.7914/SN/Z7_2010
- Roger Hansen, & Gary Pavlis. (2005). Collaborative research: St. elias erosion/tectonics project. International Federation of Digital Seismograph Networks. Retrieved from https://www.fdsn.org/networks/detail/XZ_2005/ doi: 10.7914/SN/XZ_2005
- Rufus Catchings. (2014). 2014 napa earthquake response. International Federation of Digital Seismograph Networks. Retrieved from https://www.fdsn.org/networks/detail/7C_2014/ doi: 10.7914/SN/7C_2014
- Ryberg, T., & Haberland, C. (2008). Lake toba seismic network, sumatra, indonesia. GFZ Data Services. Retrieved from http://geofon.gfz-potsdam.de/doi/network/7A/2008 doi: 10.14470/2N934755
- S. De Angelis, & A. Diaz-Moreno. (2017). Infra-etna. International Federation of Digital Seismograph Networks. Retrieved from https://www.fdsn.org/networks/detail/XF_2017/ doi: 10.7914/SN/XF_2017
- Sarah Mader, Tobias Neuffer, & Sebastian Busch. (2022). *Db miss*. International Federation of Digital Seismograph Networks. Retrieved from https://www.fdsn.org/networks/detail/1P_2022/ doi: 10.7914/SN/1P_2022
- Scripps Institution of Oceanography. (1986). Global seismograph network iris/ida. International Federation of Digital Seismograph Networks. Retrieved from https://www.fdsn.org/networks/detail/II/ doi: 10.7914/SN/II
- Servicio Geológico Colombiano. (1993). Red sismologica nacional de colombia. International Federation of Digital Seismograph Networks. Retrieved from https://www.fdsn.org/networks/detail/CM/ doi: 10.7914/SN/CM
- Servicio Sismológico Nacional, Instituto de Geofísica, Universidad Nacional Autónoma de México, México. (2017). Mx. Servicio Sismológico Nacional, Instituto de Geofísica, Universidad Nacional Autónoma de México, México. Retrieved from http://www.ssn.unam.mx doi: 10.21766-ssnmx-sn-mx
- Silvio De Angelis. (2018). Experiment in fuego. International Federation of Digital Seismograph Networks. Retrieved from https://www.fdsn.org/networks/detail/XZ_2018/ doi: 10.7914/SN/XZ_2018
- SOCQUET, A., BAEZ, J. C., MORENO, M., LANGLAIS, M., DEEP-Trigger Team, Geophysics Technical Service At ISTerre, & RESIF. (2020). Deep_trigger temporary experiment in the subduction zone peru/chile, chile (resifsismob). RESIF Réseau Sismologique et géodésique Français. Retrieved from https://seismology.resif.fr/fr/reseaux/\#/XZ_2020 doi:

10.15778/RESIF.XZ2020

- Sridhar Anandakrishnan. (1995). Antarctic microearthquake project, monitoring of ice stream c, west antarctica. International Federation of Digital Seismograph Networks. Retrieved from https://www.fdsn.org/networks/detail/XF_1995/ doi: 10.7914/SN/XF_1995
- Steve Day, & Frank Vernon. (1994). Peninsular range. International Federation of Digital Seismograph Networks. Retrieved from https://www.fdsn.org/networks/detail/XF_1994/ doi: 10.7914/SN/XF_1994
- Steve Grand, & Jim Ni. (2006). Mapping the rivera subduction zone. International Federation of Digital Seismograph Networks. Retrieved from https://www.fdsn.org/networks/detail/XF_2006/ doi: 10.7914/SN/XF_2006
- Steve Grand, & Jim Ni. (2009). Collaborative research: Northeast china extended seismic array: Deep subduction, mantle dynamics and lithospheric evolution beneath northeast china. International Federation of Digital Seismograph Networks. Retrieved from https://www.fdsn.org/networks/detail/YP_2009/doi: 10.7914/SN/YP_2009
- Susan Bilek. (2024). Bedload monitoring flume test. International Federation of Digital Seismograph Networks. Retrieved from https://www.fdsn.org/networks/detail/6E_2024/ doi: 10.7914/Y85B-6956
- Sylvie Leroy. (2003). *Dhofar seismic experiment*. International Federation of Digital Seismograph Networks. Retrieved from https://www.fdsn.org/networks/detail/XZ_2003/ doi: 10.7914/SN/XZ_2003
- Thrastarson, S., Van Herwaarden, D.-P., Noe, S., Josef Schiller, C., & Fichtner, A. (2024, June). REVEAL: A Global Full-Waveform Inversion Model. Bulletin of the Seismological Society of America, 114(3), 1392-1406. Retrieved 2025-02-18, from https://pubs.geoscienceworld.org/bssa/article/114/3/1392/637892/REVEAL-A-Global-Full-Waveform-Inversion-Model doi: 10.1785/0120230273
- Tiberi, C., Gautier, S., & RESIF. (2020). Hazard in tanzanian rift: Hatari (resifsismob). RESIF Réseau Sismologique et géodésique Français. Retrieved from https://seismology.resif.fr/networks/\#/XF__2018 doi: 10.15778/RESIF.XF2018
- Tilmann, F., Heit, B., Moreno, M., & González-Vidal, D. (2021). Anillo. GFZ Data Services. Retrieved from https://geofon.gfz-potsdam.de/doi/network/Y6/2020 doi: 10.14470/L17575324477
- Tulane University, Louisiana State University, & University Louisiana Lafayette. (2019). Induced seismicity in louisiana. International Federation of Digital Seismograph Networks. Retrieved from https://www.fdsn.org/networks/detail/Z7_2019/ doi: 10.7914/SN/Z7_2019
- Universidad de Chile. (2012). Red sismologica nacional. International Federation of Digital Seismograph Networks. Retrieved from https://www.fdsn.org/networks/detail/C1/ doi: 10.7914/SN/C1
- University of Nevada, Reno. (1971). Nevada seismic network. International Federation of Digital Seismograph Networks. Retrieved from https://www.fdsn.org/networks/detail/NN/ doi: 10.7914/SN/NN
- University of Oregon. (1990). Pacific northwest seismic network university of oregon. International Federation of Digital Seismograph Networks. Retrieved from https://www.fdsn.org/networks/detail/UO/doi: 10.7914/SN/UO
- University of Puerto Rico. (1986). Puerto rico seismic network & puerto rico strong motion program. International Federation of Digital Seismograph Networks. Retrieved from https://www.fdsn.org/networks/detail/PR/ doi: 10.7914/SN/PR
- University of Washington. (1963). Pacific northwest seismic network university of washington. International Federation of Digital Seismograph Networks. Retrieved from https://www.fdsn.org/networks/detail/UW/ doi:

- 10.7914/SN/UW
- USGS Alaska Anchorage. (2000). Usgs northern mariana islands network. International Federation of Digital Seismograph Networks. Retrieved from https://www.fdsn.org/networks/detail/MI/doi: 10.7914/SN/MI
- Utrecht University (UU Netherlands). (1983). Nars. International Federation of Digital Seismograph Networks. Retrieved from https://www.fdsn.org/networks/detail/NR/doi: 10.7914/SN/NR
- Various Institutions. (1965). International miscellaneous stations. International Federation of Digital Seismograph Networks. Retrieved from https://www.fdsn.org/networks/detail/IM/ doi: 10.7914/VEFQ-VH75
- Vergne, J., Doubre, C., & Leroy, S. (2014). Seismic network 7c:dora experiment (resif-sismob). RESIF Réseau Sismologique et géodésique Français. Retrieved from https://seismology.resif.fr/networks/\#/7C_2009 doi: 10.15778/RESIF.7C2009
- Vergne, J., & RESIF. (2021). Rittershoffen (bas-rhin, france) dense nodal seismic array temporary experiment (resif-sismob). RESIF Réseau Sismologique et géodésique Français. Retrieved from https://seismology.resif.fr/networks/\#/Z7_2018 doi: 10.15778/RESIF.Z72018
- Weisen Shen. (2023). Career: A comprehensive seismic investigation to the crust and uppermost mantle beneath the south pole, east antarctica. International Federation of Digital Seismograph Networks. Retrieved from https://www.fdsn.org/networks/detail/Y6_2023/ doi: 10.7914/TVW3-C709
- Wenyuan Fan, Yihe Huang, & S. Shawn Wei. (2018). Lake-induced earthquakes in lake erie. International Federation of Digital Seismograph Networks. Retrieved from https://www.fdsn.org/networks/detail/7D_2018/ doi: 10.7914/SN/7D_2018
- Wes Thelen, & Paul Bodin. (2009). Yakima landslide ramp. International Federation of Digital Seismograph Networks. Retrieved from https://www.fdsn.org/networks/detail/7D_2009/ doi: 10.7914/SN/7D_2009
- Yuan, X., Schurr, B., Haberland, C., Abdybachaev, U., & Sharshebaev, A. (2019).

 Multi-scale imaging of the main pamir thrust faults within the framework of
 catena project climatic and tectonic natural hazards in central asia. GFZ
 Data Services. Retrieved from https://geofon.gfz-potsdam.de/doi/
 network/7A/2019 doi: 10.14470/2N7564774946
- Zhao, L., Paul, A., Solarino, S., & RESIF. (2016). Seismic network yp: Cifalps temporary experiment (china-italy-france alps seismic transect). RESIF Réseau Sismologique et géodésique Français. Retrieved from https://seismology.resif.fr/networks/\#/YP_2012 doi: 10.15778/RESIF.YP2012
- Zhou, Y., Nolet, G., Dahlen, F. A., & Laske, G. (2006). Global upper-mantle structure from finite-frequency surface-wave tomography. *Journal of Geophysical Research*, 111 (B04304). Retrieved 2020-08-04, from http://doi.wiley.com/10.1029/2005JB003677 doi: 10.1029/2005JB003677